# Voxelwise genome-wide association study (vGWAS)

**Jason L. Stein**[a], **Xue Hua**[a], **Suh Lee**[a], **April J. Ho**[a], **Alex D. Leow**[a,b], **Arthur W. Toga**[a], **Andrew J. Saykin**[c], **Li Shen**[c], **Tatiana Foroud**[d], **Nathan Pankratz**[d], **Matthew J. Huentelman**[e], **David W. Craig**[e], **Jill D. Gerber**[e], **April N. Allen**[e], **Jason J. Corneveaux**[e], **Bryan M. DeChairo**[f], **Steven G. Potkin**[g], **Michael W. Weiner**[h,i], and **Paul M. Thompson**[a,*] **the Alzheimer's Disease Neuroimaging Initiative**

[a]Laboratory of Neuro Imaging, Department of Neurology, UCLA School of Medicine, Neuroscience Research Building 225E635 Charles Young Drive, Los Angeles, CA 90095-1769, USA

[b]Resnick Neuropsychiatric Hospital at UCLA, Los Angeles, CA, USA

[c]Center for Neuroimaging, Department of Radiology, Indiana University School of Medicine, Indianapolis, IN, USA

[d]Department of Medical and Molecular Genetics, Indiana University School of Medicine, Indianapolis, IN, USA

[e]The Translational Genomics Research Institute, Phoenix, AZ, USA

[f]Neuroscience, Molecular Medicine, Pfizer Global R and D, New London, CT, USA

[g]Department of Psychiatry and Human Behavior, University of California, Irvine, Irvine, CA, USA

[h]Departments of Radiology, Medicine and Psychiatry, UC San Francisco, San Francisco, CA, USA

[i]Department of Veterans Affairs Medical Center, San Francisco, CA, USA

## Abstract

The structure of the human brain is highly heritable, and is thought to be influenced by many common genetic variants, many of which are currently unknown. Recent advances in neuroimaging and genetics have allowed collection of both highly detailed structural brain scans and genome-wide genotype information. This wealth of information presents a new opportunity to find the genes influencing brain structure. Here we explore the relation between 448,293 single nucleotide polymorphisms in each of 31,622 voxels of the entire brain across 740 elderly subjects (mean age ±s.d.: 75.52±6.82 years; 438 male) including subjects with Alzheimer's disease, Mild Cognitive Impairment, and healthy elderly controls from the Alzheimer's Disease Neuroimaging Initiative (ADNI). We used tensor-based morphometry to measure individual differences in brain structure at the voxel level relative to a study-specific template based on healthy elderly subjects. We then conducted a genome-wide association at each voxel to identify genetic variants of interest. By studying only the most associated variant at each voxel, we developed a novel method to address the multiple comparisons problem and computational burden associated with the unprecedented amount of data. No variant survived the strict significance criterion, but several genes worthy of further exploration were identified, including *CSMD2* and *CADPS2*. These genes have high relevance to brain structure. This is the first voxelwise genome wide association study to our knowledge, and offers a novel method to discover genetic influences on brain structure.

*Corresponding author. Fax: +1 310 206 5518. thompson@loni.ucla.edu (P. M. Thompson).

## Introduction

A key goal in imaging neuroscience is to discover specific genetic variants that influence brain structure and function (Glahn et al., 2007a; Glahn et al., 2007b). The dynamic trajectory of brain development and aging throughout life is strongly influenced by genetic factors, and genetic variants have been discovered that increase risk the for Alzheimer's disease (Corder et al., 1993), other mental illness, (Gottesman and Gould, 2003; Meyer-Lindenberg and Weinberger, 2006; Purcell et al., 2009) and even obesity (Frayling et al., 2007; Ho et al., submitted for publication). The goals are both scientific and practical: by selecting those at genetic risk for early treatment, drug trials will be better powered to detect treatment effects (Frisoni et al., in press). A more mechanistic understanding of mental illness will be achieved if gene variants over-represented in patients are studied both at the molecular level and in terms of their effects on brain structure.

Early neuroimaging studies of twins found that several aspects of brain structure are under strong genetic control (Thompson et al., 2001; Posthuma et al., 2002) and that common sets of genes may influence brain structure and cognition (Posthuma et al., 2002). These "first-generation" studies estimated the relative influence of genetic contributions from relatives or family members, based on the expected genetic similarity among different types of relatives. Studies of identical and fraternal twins, and their siblings, have consistently identified heritable aspects of brain structure (Thompson et al., 2001; Styner et al., 2005; Hulshoff Pol et al., 2006; Peper et al., 2007; Schmitt et al., 2008; Brun et al., 2009; Chou et al., 2009). Except for the genotyping necessary to confirm the zygosity of twins in these studies, specific variations at the DNA level are not used in these analyses.

Early studies that use more detailed genotype information focus on specific candidate gene effects on brain structure. Several studies of candidate genes such as *APOE*, *COMT*, and *BDNF* have divided populations into carriers and non-carriers of risk polymorphisms within these genes, and detected systematic differences in brain structure using a standard statistical comparison of two groups (Egan et al., 2001; Pezawas et al., 2004; Hua et al., 2008; Chiang et al., 2009).

More recently, the second generation of studies has used genome-wide scans to search the entire genome for genetic polymorphisms that influence brain structure. In Stein et al. (submitted for publication), a common variant in the *GRIN2B* glutamate receptor gene was found to be over-represented in Alzheimer's disease and was associated with ~1.5% lower temporal lobe volume per risk allele in the elderly ($N$=742 subjects; $P<5\times10^{-7}$). Genome-wide searches have not generally been the most efficient or feasible approach in imaging genetics, as they require large samples of subjects to discover gene effects that survive stringent multiple comparisons corrections for searching over the entire genome. However, several international efforts are now underway to scan genotyped healthy and diseased subjects with the goal of discovering which genetic variants contribute to brain architecture (Thompson and Martin, 2010).

Perhaps surprisingly, no genome-wide study of brain images has used the armory of statistical methods that are now standard in human brain mapping, such as statistical parametric mapping (Friston et al., 1994; Frackowiak, 2004). One study has looked at statistical power for statistical parametric mapping with simulated genome-wide data (Hayasaka, 2009), but no experimental whole-brain whole-genome approach has been implemented to our knowledge. Most twin morphometric studies still break up the brain into subvolumes (Schmitt et al., 2007) and run genetic analysis on the numerical summaries (subvolumes).

By contrast, voxel-based morphometric approaches can make detailed 3D images of volume differences throughout the brain, without the need to specify *a priori* regions of interest or time

consuming manual tracing of anatomy in brain images. These maps of individual differences in brain morphometry make it possible to create detailed maps of gene and environmental effects on the brain, identifying spatially-varying patterns of genetic control that may not be evident if the images were summarized using a few summary indices. Maps of genetic influences on cortical anatomy reveal strong genetic control of frontal anatomy (Thompson et al., 2001), and regionally-varying gene effects (Panizzon et al., 2009). Genetic maps based on tensor-based morphometry suggest that there may be some gradients in the degree of genetic influence, with earlier developing occipital lobe structures showing stronger genetic control than frontal brain regions that mature over a more protracted developmental time-course (Brun et al., 2009; Lee et al., submitted for publication).

Here we extend the notion of statistical parametric mapping, using voxel-based methods, to include genome-wide association (GWAS) data in large populations. The result may be termed voxelwise GWAS (or vGWAS). GWAS is usually applied to study a single trait, such as IQ or the diagnosis of a specific disease, but here it is applied at each location in a brain image. The result is a 3D map of the specific genetic variants that have the greatest statistical effect in accounting for volume variations in each part of the brain, and a method to assess their statistical significance.

Recent advances in neuroimaging and genetics have made it possible, and financially feasible, to scan populations with multi-modality brain imaging and collect genome-wide data (Toga, 2002; McCarthy et al., 2008). The Alzheimer's Disease Neuroimaging Initiative (ADNI) has recently acquired genome-wide genotype data as well as structural MRI scans of 740 subjects (Mueller et al., 2005). This wealth of data is a blessing and a burden: 448,293 genotypes and 31,622 voxels in the brain in each of 740 subjects present powerful and previously unknown spatial and genetic resolution to detect specific variants that influence the brain. However, this vast amount of data requires new ways to deal with the computational load and account statistically for multiple comparisons. A genetic association is usually conducted by performing a linear regression of a phenotype on each genotype of interest, controlling for other confounding variables of no interest. Generally, a genome-wide association study examines only a few phenotypes of interest (Wellcome Trust Case Control Consortium, 2007; Sabatti et al., 2009). When conducting a voxelwise genome-wide association study, each voxel represents a phenotype, so a regression must be run at each voxel and at each SNP ($\sim 1.4 \times 10^{10}$ tests), which requires large amounts of computation time (years) if run serially on one computer. Parallelizing this process across a computing cluster can ease the computational burden, giving results in a reasonable amount of time (days). Additionally, by conducting many statistical tests (in this case $\sim 1.4 \times 10^{10}$) on the same dataset, we are highly prone to false-positive findings (Curran-Everett, 2000). Finding a method to determine only those genetic hits that are interesting to pursue without overlooking those with potentially important effects is a difficult question explored further here.

For the first time, we conducted a voxelwise genome-wide association study (vGWAS) in 740 subjects to discover genes influencing brain structure across the entire brain. Each genetic variant identified is a potential candidate with the ability to effect brain structure. If these brain traits lie on the path from genes to disorders that involve the brain (Gottesman and Gould, 2003), they could represent candidates for further study in neurological and psychiatric diseases.

## Materials and methods

### Sample

Neuroimaging and genetic data were acquired from 818 subjects as part of the Alzheimer's Disease Neuroimaging Initiative (ADNI), a large 5-year study launched in 2003 by the National

Institute on Aging (NIA), the National Institute of Biomedical Imaging and Bioengineering (NIBIB), the Food and Drug Administration (FDA), private pharmaceutical companies, and non-profit organizations, as a $60 million, public-private partnership. The goal of the ADNI study is to determine biological markers of Alzheimer's disease through neuroimaging, genetics, neuropsychological tests and other measures in order to develop new treatments, monitor their effectiveness, and lessen the time of clinical trials. The Principal Investigator of this initiative is Michael W. Weiner, M.D., VA Medical Center and University of California – San Francisco. Subjects were recruited from 58 sites in the United States. The study was conducted according to the Good Clinical Practice guidelines, the Declaration of Helsinki, and U.S. 21 CFR Part 50—Protection of Human Subjects, and Part 56—Institutional Review Boards. Written informed consent was obtained from all participants before protocol-specific procedures were performed. All data acquired as part of this study are publicly available (http://www.loni.ucla.edu/ADNI/).

All subjects underwent thorough clinical and cognitive assessment at the time of scan acquisition to determine diagnosis. The mini-mental state exam (MMSE) was administered to provide a global measure of mental status (Cockrell and Folstein, 1988). The clinical dementia rating (CDR) was used to assess dementia severity (Morris, 1993). Healthy volunteer status was determined through MMSE scores between 24 and 30 (inclusive), a CDR of 0, non-depressed, non-MCI, and non-demented. MCI diagnosis was determined by MMSE scores between 24 and 30 (inclusive), a memory complaint, objective memory loss measured by education adjusted scores on the Wechsler Memory Scale Logical Memory II, a CDR of 0.5, absence of significant levels of impairment in other cognitive domains, essentially preserved activities of daily living, and an absence of dementia. Diagnosis of AD was made according to NINCDS-ADRDA criteria for probable AD (McKhann et al., 1984), MMSE scores between 20 and 26 (inclusive), and CDR of 0.5 or 1.0.

Population stratification is a known problem in genetic association analyses, which can produce false-positive or false-negative results (McCarthy et al., 2008). When multiple subpopulations are present in the data (population stratification), spurious associations (or lack of associations) can result from allele frequency differences between populations rather than associations with the phenotype (Lander and Schork, 1994). 818 subjects were genotyped as part of the ADNI study. However, only unrelated Caucasian subjects (non-Hispanic; $N$=740) identified by self-report and confirmed by MDS analysis (see Stein et al., submitted for publication) were included to reduce population stratification effects. Volumetric brain differences were assessed in 173 AD patients (78 female/95 male; mean age±standard deviation=75.54±7.66), 361 MCI subjects (130 female/231 male; 75.16±7.29), and 206 healthy elderly subjects (112 male/94 female; 76.13±4.94). The genome-wide analyses were not split into diagnostic groups as the goal was to present as broad a phenotypic continuum (Petersen, 2000) as possible, to provide the highest power to detect genetic associations.

## MRI analysis methods

3D $T_1$-weighted baseline brain MRI scans were analyzed using tensor-based morphometry (TBM) as detailed in a previous study (Hua et al., 2008). Briefly, high-resolution structural brain MRI scans were acquired at 58 ADNI sites with 1.5 T MRI scanners using a sagittal 3D MP-RAGE sequence developed for consistency across sites (Jack et al., 2008) (TR=2400 ms, TE=1000 ms, flip angle=8°, field of view=24 cm, final reconstructed voxel resolution=0.9375× 0.9375×1.2 mm$^3$). Images were calibrated with phantom-based geometric corrections to ensure consistency across scanners. Additional image corrections included (Jack et al., 2008): (1) correction of geometric distortions due to gradient non-linearity, (2) adjustment for image intensity inhomogeneity due to B1 field non-uniformity using calibration scans, (3) reducing residual intensity inhomogeneity, and (4) geometric scaling according to a phantom scan

acquired for each subject to adjust for scanner- and session-specific calibration errors. Images were linearly registered with 9 parameters to the International Consortium for Brain Imaging template (ICBM-53) (Mazziotta et al., 2001) to adjust for differences in brain position and scaling.

For TBM analysis, the protocol was identical to that of a prior study analyzing the clinical correlates of temporal lobe atrophy (Hua et al., 2008) in a smaller population; since then, genome-wide genotype data was collected. First, a minimal deformation template (MDT) was created for the healthy elderly group to serve as an unbiased average template image to which all other images were warped using a nonlinear inverse-consistent elastic intensity-based registration algorithm (Leow et al., 2005). Volumetric tissue differences were assessed at each voxel in all individuals by calculating the determinant of the Jacobian matrix of the deformation, which encodes local volume excess or deficit relative to the mean template image. The map of volumetric tissue differences were then down-sampled using trilinear interpolation to $4 \times 4 \times 4$ mm$^3$ isotropic voxel resolution for computational efficiency. This percentage volumetric difference relative to a population-based brain template at each voxel served as a quantitative measure of brain tissue volume difference for genome-wide association.

### DNA isolation and SNP genotyping methods

DNA was isolated from B lymphocytes cells taken from blood (Neitzel, 1986) and extracted (Lahiri et al., 1992) using standard procedures. 7 ml of EDTA blood was extracted using the QIAamp DNA Blood Maxi Kit (Qiagen, Inc., Valencia, CA). Samples were processed according to the manufacturer's protocol. Genomic DNA samples were analyzed on the Human610-Quad BeadChip (Illumina, Inc. San Diego, CA) according to the manufacturer's protocols (Infinium HD Assay; Super Protocol Guide; Rev. A, May 2008). Before initiation of the assay, 50 ng of genomic DNA from each sample was examined qualitatively on a 1% Tris-acetate-EDTA agarose gel for visual signs of degradation. Any degraded DNA samples were excluded from further analysis. Samples were quantitated in triplicate with PicoGreen® reagent (Invitrogen, Carlsbad, CA) and diluted to 50 ng/µl in Tris-EDTA buffer (10 mM Tris, 1 mM EDTA, pH 8.0). 200 ng of DNA was then denatured, neutralized, and amplified for 22 h at 37 °C (this is termed the MSA1 plate). The MSA1 plate was then fragmented with FMS reagent (Illumina) at 37 °C for 1 h and then precipitated with 2-propanol and incubated at 4 °C for 30 min. The resulting blue precipitate was then resuspended in RA1 reagent (Illumina) at 48 °C for 1 h. The samples were then denatured (95 °C for 20 min) and immediately hybridized onto BeadChips at 48 °C for 20 h. BeadChips were then washed and subjected to single base extension and staining. Finally, the BeadChips were coated with XC4 reagent (Illumina), dessicated, and imaged on the BeadArray Reader (Illumina).

### Genetic analysis

Genome-wide genotype information was collected at 620,901 markers. Multiple types of genetic variants were genotyped, but only Single Nucleotide Polymorphisms (SNPs) were included in this analysis. Alleles on the forward strand are reported. Individual markers were excluded from the analysis that did not satisfy the following quality criteria based on previous genome-wide association studies (Wellcome Trust Case Control Consortium, 2007): genotype call rate <95% (42,670 SNPs removed), significant deviation from Hardy–Weinberg equilibrium $P<5.7 \times 10^{-7}$ (871 markers removed), minor allele frequency <0.10 (161,354 SNPs removed), and a platform-specific recommended quality control score of <0.15 (variable number of SNPs removed across subjects). A minor allele frequency cut-off of 0.10 (10%) was used to ensure that sufficient numbers of subjects would be found in our sample in each genotypic group (homozygous major allele, heterozygous, homozygous minor allele) using an additive genetic model. If alleles are in Hardy–Weinberg equilibrium, a minor allele frequency cut off of 0.10 ensures that at least 7 subjects are in the smallest genotypic category. If this cut-

off is not imposed, there is a risk of findings being driven by a small number of subjects in the sample, which may be less robust to sampling effects. 448,293 SNPs remained for analysis after quality control. Missing data still occurs over these remaining SNPs, but after filtering >95% of the subjects must have a successfully genotyped SNP for it to be included.

Association was conducted using a modified version of the Plink software package (Purcell et al., 2007) (version 1.05; http://pngu.mgh.harvard.edu/purcell/plink/) to conduct a genome-wide association at each of 31,622 voxels within a whole-brain mask of the MDT across all 740 subjects. At each voxel, a regression was conducted at each SNP with the number of minor alleles, age, and sex as the independent variables and the quantitative phenotype (percentage volume difference relative to a subject specific template at each voxel) as the dependent variable, assuming an additive genetic model. To simplify and condense the large results (~140 MB) output at each voxel, the open-source Plink software was modified to only output the identifier and *P*-value of the most associated SNP (21 bytes). Each genome-wide regression required ~9 min of computation time, so the process was split for parallel computing across 300 cluster nodes using the Laboratory of Neuro Imaging (LONI) pipeline (http://pipeline.loni.ucla.edu/). The total computation time was approximately 27 h.

An additional analysis was performed to determine if spatial clustering of *P*-values occurred in a null map. Though a calculation of an extensive permutation distribution was not feasible, we conducted one permutation to get an idea of how the data on top (most significant) SNPs might look in a null distribution. The genomes, sex, and age were randomly swapped among subjects and the same analysis as above was run again. The output from this analysis is shown in Fig. 5.

Genes and ESTs (expressed sequence tags) in close proximity to significant SNPs were localized through the UCSC genome browser (Kent et al., 2002) (http://genome.ucsc.edu/) and are reported in Table 2. Additionally, gene functions and known associations with disease were reviewed using the gene ontology information from the Entrez Gene (http://www.ncbi.nlm.nih.gov/sites/entrez?db=gene) database.

### Determination of statistical threshold

Selecting only the *P*-value for the most highly associated SNP at each voxel does not give, in the null case, a usual uniform distribution of *P*-values from which to calculate the corrected significance of the findings. Because we are using only the minimum *P*-value from a set of tests of each of the genetic markers, we must find the appropriate type of null distribution to use in this situation. If *n* independent random variables $X_1, X_2, \ldots, X_n$ are uniformly distributed on the unit interval [0,1], the minimum of these variables follows the probability density function (Ewens and Grant, 2001):

$$f_{min}(x) = n(1-x)^{n-1}.$$

The PDF derived above $f_{min}(\chi)$ is a Beta distribution with parameters $\alpha=1$ and $\beta=n$. At each voxel then, the null distribution for the *P*-value of the most strongly associated SNP across *n* independent genomic markers (the minimum *P*-value) approximately follows *a Beta*(1, *n*) distribution.

It is well known, however, that all genomic markers are not independent (Frazer et al., 2007). Genetic variation is often inherited in contiguous segments of DNA, such that there tends to be correlation between the inheritance of alleles at markers close to each other on the same chromosome. This genetic correlation is called *linkage disequilibrium* (LD), and, as a result, the effective number of independent tests ($M_{eff}$) conducted is less than the total number of

markers ($M$). By effective number of tests, we mean the number of independent tests that would have to be conducted to lead to a null distribution for the minimum $P$-values that was approximately the same as that obtained when conducting tests that are necessarily correlated due to LD.

To estimate the effective number of tests conducted as part of the study, simpleM (https://dsgweb.wustl.edu/rgao/) was used (Gao et al., 2008; Gao et al., 2010). This program first derives the composite LD structure between SNPs, calculates eigenvalues through principal component analysis on the composite LD matrix, and sets $M_{eff}$ equal to the number of principal components required to jointly explain 99.5% of the variance in the SNPs. This process has been verified to give $M_{eff}$ estimates similar to those derived from a gold-standard permutation-based null distribution when applied to several commonly used SNP chips (Gao et al., 2010).

SimpleM requires that there must be no missing genotype information. Therefore, it was necessary to perform imputation of the genetic data prior to $M_{eff}$ analysis. Imputation was done using Mach (version 1.0; http://www.sph.umich.edu/csg/abecasis/MaCH/index.html) to infer the phase of the haplotype and automatically impute missing genotypes (Li et al., 2009). The parameters of Mach were set to 50 iterations of the Markov Sampler and 200 haplotypes considered when updating each individual. Each chromosome was imputed separately. Imputation was not conducted for sex chromosomes or for mitochondrial DNA. SimpleM was used on the imputed dataset, and the resulting $M_{eff}$ estimates are presented in Table 1. $M_{eff}$ was set to be equal to $M$ for sex chromosomes and mitochondrial DNA as the use of simpleM in this context has not been verified (Gao et al., 2008; Gao et al., 2010).

The effective number of tests was estimated to be 275,575, which is markedly reduced from the 448,293 markers directly measured in this experiment. A comparable reduction was reported by (Gao et al., 2010). We therefore chose to model the null distribution as $Beta$(1, 275575). Because the inter-SNP correlation depends on the number and density of SNPs examined, this distribution would need to be re-estimated for new types of genomic data, for instance if a chip with a different density were used (e.g., 1 million SNPs). To determine how well the analytic Beta distribution derived above fits the observed data, a histogram of the observed distributions is compared to PDF of the theoretical distribution in Fig. 1. Both distributions are compared directly in a Q–Q plot. The theoretical distribution fits the observed data well for the most part.

Based on the theoretical distribution of the minimum $P$-value from all genetic markers, the $P$-values from the empirical studies were then "corrected" through the cumulative distribution function (CDF) of the derived beta distribution. By adjusting the data using the CDF of the theoretical distribution, common corrections for multiple comparisons may be used on the "corrected" $P$-values ($P_c$-values). The False Discovery Rate (FDR) correction for multiple comparisons (Benjamini and Hochberg, 1995) is reliant on receiving data that has a null $P$-value distribution that is uniform on the interval [0,1] (Dabney and Storey, 2006). The minimum $P$-value distribution above clearly does not meet that criterion, but the $P_c$-value data at least approximately does, as shown in the histogram and quantile–quantile plot of the $P_c$-value distribution (Fig. 2).

### False discovery rate correction for multiple comparisons

Following correction of the raw $P$-values, a False Discovery Rate (FDR) correction for multiple comparisons may be used to estimate if there is a statistical threshold that can be applied to the maps that controls the expected rate of false-positives at a nominal rate (usually 5%) among all rejected hypotheses (Benjamini and Hochberg, 1995; Genovese et al., 2002). The FDR method for multiple comparisons correction is especially suitable for exploratory analyses like

those presented here where we search for genes affecting brain structure (Storey, 2003). Here we set the FDR to $q$=0.05, so that, on average, 95% of voxels declared significant are true positives. The maps show that our data can only be thresholded at a level that gives a false discovery rate of roughly 50%, and no statistical threshold controls the FDR at the conventional $q$=0.05 level (Fig. 3).

The original FDR method (Benjamini and Hochberg, 1995) assumes that the data for each test is statistically independent and the *P*-values are sampled from a uniform [0,1] distribution (Dabney and Storey, 2006). The data are not statistically independent as the genomic structure has linkage disequilibrium, or correlation between markers, and the neuroimaging data also has spatial smoothness. If the data have a "positive regression dependency", i.e., the test statistics of the regression are positively correlated, the Benjamini– Hochberg procedure controls the FDR successfully (Benjamini and Yekutieli, 2001). This is most likely a valid assumption for neuroimaging and genetic data (Genovese et al., 2002; Storey and Tibshirani, 2003).

The original FDR method (Benjamini and Hochberg, 1995) is the most conservative of FDR methods in that it will always control the number of false-positives among rejected hypotheses at the specified *q*-level, given independence of the data and sampling from a uniform distribution when null. Given added assumptions, though, several alternative FDR methods may be used to correct for multiple comparisons, and can give less conservative estimates of significance (Pounds, 2006). The positive False Discovery Rate (pFDR) is a modification of FDR, conditioning on one finding positive finding having occurred (i.e., one null hypothesis being rejected) (Storey, 2003). The pFDR method is implemented in the R statistics program (http://www.r-project.org/; Version 2.8.1) as the "q-value" package (Version 1.20.0), used here to calculate the *q*-values according to the pFDR method.

Several alternative methods have been proposed to correct empirical data to fit the assumptions of the FDR method (Leek and Storey, 2008), or to correct the FDR assumptions to fit the non-independence of the data (Li and Ji, 2005).

### Estimation of sample size needed for replication

To estimate how many subjects would be needed to replicate the finding that these genetic variants are associated with brain structure conditional on the dataset, we used a re-sampling approach. The most associated voxel for each of the 5 most significantly associated SNPs (see Table 2) was used as an example phenotype. For each SNP, three subjects, one from each diagnostic category (AD, MCI, and healthy control), were randomly picked and removed from the analysis and the *P*-value for each of the significant SNPs was calculated at the most associated voxel. The process was repeated until no more subjects remained in the diagnostic category with the least number of subjects (165 AD subjects). To estimate confidence intervals for this estimate, the resampling was repeated 1000 times. 95% confidence intervals were based on the 2.5th and 97.5th percentiles of the resampled distribution.

## Results

### Voxelwise GWAS results

Maps of the significance level at each voxel for the most associated SNP within that voxel were recorded and displayed in Fig. 4. There are spatially contiguous hot spots of significant association, with a "raw" minimum *P*-value of $2.56 \times 10^{-10}$ ($P_c$-value=$7.05 \times 10^{-5}$) across the entire brain. There is a certain amount of spatial clustering because all voxels are not independent so some spatial clustering is expected even if the null hypothesis were true. To get an approximation of how much spatial clustering is expected by chance, Fig. 5 shows the

minimum *P*-values in each voxel after the genomes have been randomly assigned to each subject. A certain amount of clumping is expected when top SNP maps are made from null data. One source of spatial coherence in these maps is that they are based on smooth maps of volumetric differences computed using tensor-based morphometry, which uses nonlinear image registration of each subject's imaging data to a template. These methods generate spatially smooth maps of volume differences, where the level of smoothness is dependent on the form of the regularizer (Laplacian, elastic, fluid, etc.) and also on the spatial resolution of the numerical grid used to solve the differential equations whose solution is the deformation field. In our approach, the elastic regularizer is decomposed into its eigenfunctions so that the warping fields can be computed using a Fast Fourier transform. Because these deformation fields are smooth, so are averages and differences of their Jacobian (gradient) maps, and so are the resulting statistical maps. In the future, it may be interesting to see if there is more latent structure or anatomical coherence in the top SNP maps than would be otherwise expected if the data were completely null. Even so, there may be relevant genes that influence brain structure but are never the top SNP in a map of this kind. If so, their effects might be more spatially distributed (coherent) without ever being represented in a top SNP map. Given this, clearly extensions of vGWAS might be proposed that emphasize the total extent, or cluster size, as well as the peak height of the association *P*-values, a tactic that can be more powerful than a peak height or maximum statistic (top SNP) test for detecting subtle but distributed effects of weak effect size in statistical parametric maps.

The voxelwise GWAS showed 8,212 unique SNPs which were most associated at each voxel. In other words, if the "winning SNP" was picked for each voxel, the same SNP was picked over spatially coherent regions. There does not appear to be a great deal of hemispheric symmetry in the spatial distribution of the "winning" SNP at each voxel (Fig. 6). However, the SNPs presented here do have an effect on brain volume beyond the most highly associated voxels shown. The 20 "top" SNPs with the most significant association to any voxel are shown in Table 2. The most significant SNPs were found in several genes.

The two most significantly associated SNPsin the study, rs2132683 and rs713155, are both found in intergenic regions of chromosome 6. These SNPs are the "winning SNP" at voxels located in the white matter near the left posterior lateral ventricle (rs2132683) and in the cerebral aqueduct and fourth ventricle (rs713155; Fig. 6). The allele frequency of the minor allele at rs2132683 has a trend level difference between diagnostic groups (AD and MCI: 0.339; healthy elderly: 0.291; *P*=0.0793; OR=1.25) as does rs713155 (AD and MCI: 0.416; healthy elderly: 0.347; *P*=0.016; OR=1.34).

SNP rs476463 is located within an intronic region of the *CSMD2* gene. *CSMD2* has highest expression in the brain and may be a oligodendroglioma suppressor (Lau and Scholnick, 2003), though the function of the protein is largely unstudied. Additionally, it has been associated with ADHD (Lesch et al., 2008) and addiction (Liu et al., 2006). The allele frequency of this SNP did not statistically differ between diagnostic groups (AD and MCI: 0.116; healthy elderly: 0.131; *P*=0.428; OR=0.871).

SNP rs2429582 is located within an intronic region of the *CADPS2* gene and is the SNP that associated with brain structure the most in the lateral temporal lobe. This gene regulates synaptic and large dense core vesicle priming in neurons, especially promoting monoamine uptake and storage in neurons (Brunk et al., 2009). *CADPS2* is strongly expressed in the brain, specifically in cerebellum, cortex, olfactory bulb, hippocampus, striatum, thalamus, and superior and inferior colliculi (Speidel et al., 2003). The gene is located in an area with known linkage to autism (Cisternas et al., 2003). Splice variants of this gene may also be relevant to autism (Sadakata et al., 2007), though there is some controversy over this finding (Eran et al.,

2009). The allele frequency for this SNP had a trend level difference between diagnostic groups (AD and MCI: 0.355; healthy elderly 0.307; $\chi^2$=2.989; OR=1.24).

The fifth most associated SNP in this analysis, rs9990343, is in an intergenic region of the genome on chromosome 3. It is the "winning SNP" in voxels of the superior frontal lobe (Fig. 6). The allele frequency for this SNP did not statistically differ between diagnostic groups (AD and MCI: 0.489; healthy elderly 0.461; $P$=0.341; OR=1.12).

Other genes of interest identified here are *WFDC2*, expressed in epithelial cells and thought to be involved in ovarian cancers (Bingle et al., 2002); *SPINT3*, serine peptidase inhibitor, Kunitz type 3 (Lundwall, 2007); *SHB*, involved in apoptosis, signal transduction (Lindholm, 2002), cell differentiation, and may interact with other proteins to cause neurite growth (Zhang et al., 2006); *KIAA0090* which currently has an unknown function; *MRTO4* which may be involved in mRNA turnover and ribosome assembly (Lo et al., 2009); *AKR7L* which is an aldo-keto reductase (Mindnich and Penning, 2009); *BOK* which is in a family of proteins that act as anti- and pro-apoptotic regulators (Bartholomeusz et al., 2006); *THAP4*, which does not have a known function (Roussigne et al., 2003); *RBBP6*, which encodes a retinoblas-toma tumor suppressor (Sakai et al., 1995); *FARP1*, which promotes dendritic growth (Zhuang et al., 2009); *FRMD6* and *GLYATL3* have unknown function. Additionally, SNPs were found in ESTs BG436399 and BC036700 (Strausberg et al., 2002) and BG334794.

### Statistical threshold

The statistical threshold was calculated using two methods that control the FDR on the $P_c$-values. The original FDR method (Benjamini and Hochberg, 1995), which is valid in cases of positive regression dependency (Benjamini and Yekutieli, 2001), sets a critical *P*-value significance threshold for the second-most associated SNP (rs713155), with a false discovery rate of $q$=0.50 (or ~50%) when the $P_c$-value threshold is $2.97\times10^{-4}$ (Fig. 3). The pFDR threshold gives a $q$-value of 0.25 for the most associated voxel of SNP rs2132683.

### Sample size needed for replication

Replication is crucial for any experiment, but especially so in genomic studies that have a high chance for false-positive results because so many tests are conducted. Here, we conducted a resampling approach to determine how many subjects would be needed to replicate our findings with 95% confidence (Fig. 7). This resampling procedure shows that an independent sample of fewer than 312 subjects for rs2132683, 263 subjects for rs713155, 291 subjects for rs476463, 299 subjects for rs2429582, and 319 subjects for rs9990343 would be required to replicate the effects shown here with 95% confidence in a new sample at a significance level of $P < 0.01$ (a nominal $P < 0.05$, Bonferroni corrected for five independent tests). We note that the standard $P < 0.05$ level rather than the genome-wide significance would be applicable to a replication sample, as a prior hypothesis regarding the specific gene variant exists. In general, it seems desirable for imaging genetics studies to estimate the sample size needed to replicate a given finding, and to rank them for different findings, so that promising leads can be followed with maximum efficiency. In the imaging genetics community, it may also be possible to facilitate data sharing through the ENIGMA (Thompson and Martin, 2010) network (http://enigma.loni.ucla.edu/) sufficient to replicate a finding if the sample size required is known. The tables of "top SNPs" may then be shared with useful estimates of the sample sizes needed for replication.

## Discussion

### Methodological overview

Here we present a method to conduct a voxelwise genome-wide association study (vGWAS). In summary: (1) we conducted a genome-wide association analysis using volume differences relative to a mean brain image template at each voxel as a phenotype, after controlling statistically for age and sex; (2) we selected only the most associated voxel, saving its *P*-value and identifier; (3) the effective number of tests was calculated through determination of the number of principal components that describe 99.5% of the genotypic variance; (4) the *P*-value was corrected across SNPs through a transformation using the CDF of an analytic *Beta* distribution with parameter estimated by the effective number of tests; and (5) the $P_c$-value maps were assessed for how they controlled the false discovery rate, using various implementations of the FDR theory to correct for multiple comparisons.

Overall, no SNPs survived FDR correction at the conventional *q*=0.05 threshold, but several interesting genes were identified that already have a known mechanistic relation to brain structure or to specific diseases of the brain, making them worthy of attempting replication.

### Assumptions of model

This method defined above is equivalent to a "winner-take-all" map for SNPs, where the most associated SNP is represented in each voxel. Our method is losing information by only looking at one SNP per voxel, but even this data reduction technique requires novel analysis methods and extensive computational time. Other methods have been proposed to assess the simultaneous effects of multiple SNPs across multiple voxels, such as multivariate principal or independent component analysis (Liu et al., 2009). In addition, canonical correlation analysis (CCA) (Hotelling, 1935, 1936; Lee et al., submitted for publication), could be used to seek an optimal basis (or linear combination) for two high-dimensional vectors (i.e., the images and the SNP set), to maximize their correlation or mutual information. This basis can then be used to determine the maximum correlations between the two datasets, by diagonalizing the total covariance matrix between the vectors (Fillard et al., 2005). CCA, and its nonlinear variants such as kernel CCA and adaptive boosting, are especially attractive as they could be used to find optimal image projections that maximally correlate with subsets of genes. A region of an image, with specific weights derived from CCA, could then become a candidate phenotype of interest. This multivariate correlation method has been adapted already to seek genetic influences on 6-dimensional diffusion tensors in twins, without throwing away the substantial information in the diffusion tensor by dimension reduction (Lee et al., submitted for publication). Even so, the extension of these multivariate correlation methods to genome-wide data has not been explored and would require a great deal of memory.

Both the *Beta* transformation and FDR correction for multiple comparisons work under the assumption of independence (or positive dependence in the case of FDR). This assumption of independence is not precisely true for neuroimaging or genetic data. Neuroimaging data has spatial smoothness due to both scan acquisition and analysis parameters. The smoothness of the Jacobian maps that are derived from TBM analysis is partially determined by pre-specified registration parameters that affect the spatial covariance (Green's function) in the 3D deformation vector fields that are used to measure volumetric differences. These Green's functions can be set adaptively, in principle, and can be considered equivalent to spectral or neural network model of neuroanatomical variation that may be estimated from the data rather than specified analytically (Grenander and Miller, 1998; Fillard et al., 2005). Because of this, some spatial autocorrelations (spatial coherences) in the maximum SNP map are expected even when null (Fig. 5). Similarly, because genetic variation is inherited in contiguous segments of DNA due to recombination happening often in specific locations, there is a great deal of

correlation between genetic markers recorded here, which is taken into account through calculation of $M_{eff}$ (Table 1).

A common method to correct for multiple comparisons taking into account non-independence of the data is to calculate exact *P*-values by shuffling labels, in this case genetic variation and voxels, between subjects. By doing this many times, a true null distribution is developed which automatically accounts for the spatial and genetic correlations in the sample. Unfortunately, with data sets this large it is not computationally feasible to calculate a null distribution through resampling in a reasonable amount of time. Each analysis takes 27 h to complete even when parallelized across 300 computing nodes, so a resampling with only 1000 permutations would take ~3 years.

Permutation tests are the gold standard for calculating significance levels and determining $M_{eff}$. As mentioned above, permutation tests are not computationally feasible here, so we used a quick and effective method for determining $M_{eff}$. Using a measure of the effective number of independent tests is controversial (Nichols and Hayasaka, 2003; Dudbridge and Koeleman, 2004). Previous work has shown that when calculating the effective number of tests conducted, the calculated distribution was significantly different from a permutation-derived distribution (Dudbridge and Koeleman, 2004). However, a different algorithm is used here for determining the effective number of tests (simpleM) and was found to match very well with the effective number of independent tests fit to a *Beta* distribution of permuted data in two datasets (Gao et al., 2010). Other work has shown that in neuroimaging data, the effective number of independent tests does not match that of a permuted dataset when there is high spatial smoothness (local autocorrelation) in the residuals of the dataset after statistical model fitting (Nichols and Hayasaka, 2003). However, here we use the effective number of tests to correct across the genetic data, an application where the procedure has been shown to give accurate results in comparison to a gold-standard permuted null dataset (Gao et al., 2010).

### Validity of the beta distribution and effects of violations of distributional assumptions

Serious consideration must be given to how violations of the assumptions of the *Beta* transformation might affect the results of the analyses. In fact, if null data deviates from a *Beta* distribution (e.g., in the tails) will impact some steps of the analysis (the FDR correction, which is based on significance) but not others (the ranking of the SNPs and the top SNP map). The goal of the $Beta(1, M_{eff})$ method of adjusting the raw *P*-values is "uniformization" of the $P_c$-values under the null hypothesis. In other words, if the data are truly null, then the $P_c$-values should approximately follow a uniform distribution on the unit interval [0,1]. In Figs. 1 and 2, the Q–Q plots show the approximate fit to the $Beta(1, M_{eff})$ distribution in the bulk regime (i.e. where the effect sizes are lowest), but in the tail, there may be deviations from the fit. True positives would induce such deviations, but an inappropriate fit could also do this. In simulations with correlated Gaussian samples, a $Beta(1, M_{eff})$ fit does well in the bulk, but there are deviations from uniformity for small $P_c$-values (we acknowledge an anonymous reviewer for noting this). Such deviations will not affect the SNP ranking, as any conversion from *P* to $P_c$ is monotonic. However, they would affect the significance testing. Although FDR applied to the images here did not give a significant finding, so the point does not affect the conclusions drawn, if the $P$-to-$P_c$ is used as the basis for significance testing, its empirical fit should be tested more thoroughly and perhaps modified based on a partially permuted dataset, where feasible.

### Methods to increase power in vGWAS

First, minimal N plots (Fig. 7) estimate, through a resampling procedure, how many subjects might be needed to replicate a finding. These SNPs could be validated by conducting a similar experiment in a new sample, looking at only the SNPs of interest at the voxels or regions found

here. By reducing the number of comparisons (fewer voxels and fewer SNPs), a less stringent statistical threshold is needed for comparison because fewer tests are conducted.

This minimal N analysis differs from experiments which do not reject the null hypothesis, and then attempt to determine the experimental power to reject the null. The idea of a post-hoc power calculation has been shown to be fallacious (Hoenig and Heisey, 2001; Levine and Ensom, 2001) and is not the goal here. Instead we look to estimate, approximately, the reduced number of subjects that might be needed to replicate our results in a separate experiment. Using an initial sample to determine the number of subjects needed to replicate a finding in a completely independent sample does not have the same fallacy of the post-hoc power calculation which attempts to calculate the power to achieve significance on the same sample. The goal of the analysis presented is to determine how many subjects are needed to pass a lower replication significance threshold. If the finding is true, and if the sample here is representative of the population, 95% of the time in new experiments the SNP will be significant at a replication threshold.

Notably, because vGWAS does lead to restricted regions of interest for associations, future studies could take advantage of the limited search region to specify a region of interest, increasing power by eliminating false-positive voxels. The selection of statistically-defined regions of interest has been useful in other large voxel-based morphometry studies. For example, in a study of 515 ADNI subjects scanned twice, Hua et al. (2009) found that the sample sizes needed to find drug effects on the rates of brain atrophy were drastically reduced if the analysis focused on voxels that had shown strong effects sizes in a small independent training sample. Summary measures from this statistical region of interest were more powerful than those based on atlas-based anatomic criteria, suggesting the benefit of voxel-based methods, at least in some cases, over anatomical parcellation.

To implement such an approach, one could use two datasets: one for training and one for testing. The training dataset could be trained to specify areas of greatest heritability or areas of greatest genetic association. These areas could then be used as "training" ROIs to search for genetic influence. Using vGWAS, the most associated SNPs at the most associated voxels could be used as "testing" ROIs where we would expect much higher power in the "testing" dataset, as fewer voxels and fewer SNPs are tested for association. The ADNI study has used this method successfully to increase power to detect changes with greatest statistical effect sizes in AD (Hua et al., 2009; Ho et al., in press). Genetics studies have also advocated this multi-stage approach to maximize power with reduced genotyping cost (Skol et al., 2006).

Additionally, machine learning algorithms such as support vector machines (Burges, 1998) or Adaboost (Freund and Schapire, 1997; Morra et al., 2008) could offer a method to identify the most powerful phenotype, that is a set of voxels, and an associated set of weights, with the greatest power to associate with genetic variation. A linear version of this approach is canonical correlation analysis; a nonlinear version might use machine learning methods such as kernel CCA, support vector machines, or boosting (Morra et al., 2009). If the performance of this system were high on new data, one could use the new classifier output as the endophenotype (Sun et al., 2009) and regress it against genetic variation using standard association software, such as Plink.

Conversely, machine learning methods could be used to find gene sets or networks that best predict the image value (Gu et al., 2009). In this way, one would be directly building a genetic model for the data. The gene set could be limited to the best candidates from the training/ screening phase of the data as detailed above. This could motivate a design where one detrends the effects of the top SNPs when looking for others. Adaptive boosting could be applied to this problem, as it could fit a powerful weighted model ranking the top SNPs even if they each had

a small effect (similar to "weak learners", in terminology of machine learning) (Morra et al., 2009).

## Biological significance of the findings

Genome-wide association using brain phenotypes in humans has only been started in a few previous studies, to our knowledge (Seshadri et al., 2007; Potkin et al., 2009a; Potkin et al., 2009b). These studies used data reduction techniques by only studying gross phenotypes of interest like total cranial, lobar, ventricular, or hippocampal volumes. Our analysis offers a conceptual advantage as it searches for voxelwise genetic associations in 3D, which should offer much greater anatomical detail about genomic association, with potentially higher statistical power. Using this method, we found several genes with high relevance to brain structure. Specifically, *CADPS2* is involved with monoamine uptake in neurons; *CSMD2* and *CADPS2* have been associated with psychiatric illness; and *SHB* and *FARP1* are associated with neurite growth. Given this prior information on how these genes function on the brain, it is likely that some of the genetic variants found here have important effects on the structure of the brain. Many other genes have not been well-studied or characterized so may well have an effect on brain structure.

In Fig. 6, many of the locations of greatest association beyond any other SNP for the 5 most associated SNPs are near a significant edge in the brain—next to the brain surface, major fissure, or ventricles. It is worth considering whether such a localization may be due to a bias (differential sensitivity) that might arise from the method of image warping followed by using the warp's Jacobian determinant as the dependent variable. If statistical maps based on deformation fields tended to detect effects more frequently at edges than in the rest of the brain, then this would be a possible source of bias, but it appears not to be the case in other empirical studies using TBM (in fact the opposite tends to be the case). Most studies with deformation morphometry tend to show the greatest effect sizes throughout large homogeneous regions, and notably our TBM studies of Alzheimer's disease find greatest effects in broad regions of the brain's white matter, or throughout the lateral ventricles, both at 1.5 T and 3T, and in large samples (Hua et al., 2009;Ho et al., in press). Also, statistical effects are not preferentially detected at edges in images when the effects of single candidate genes on the brain are assessed with TBM (Ho et al., submitted for publication). Although the deformation is driven by a body force (image gradient, or variational derivative of a cost function) that is generally greatest at the edges of structures in the images, the interiors of structures still tend to be better registered than their boundaries once all the data are aligned. In the interiors of structures, coherent patterns (such as atrophy) are more likely to be reinforced across all members of a group than at boundary voxels that may be less well registered across all subjects in the group, even after nonlinear registration. After all, the registration algorithm focuses on improving the alignment of edges as they are always the least well registered parts of the image, and therefore these regions are likely to show low effect sizes in a population study. Even so, some warping methods use regularizers that are designed to make the Jacobian determinant as uniform as possible in regions of homogeneous image intensity (e.g., the sKL-MI method, see Yanovsky et al., (2009)), so the Jacobian determinant will change the most at an image edge. If this is true, and if the "top SNP" is a different SNP for different structures, then it is more likely that the top SNP in a vGWAS map will change at the boundary of a structure. This is speculative, and the spatial coherence of top-SNP maps may depend on the sample size, the true spatial correlation in the "top SNP" maps in an arbitrarily large sample, as well as the methods (maximum statistic vs. cluster size statistic) used to detect them. The spatial correlation for single gene effects on brain structure can be quite large, in TBM studies of candidate genes that influence brain structure (Ho et al., submitted for publication).

As in other ADNI analyses, we did not covary for medication status of the subjects. It cannot be absolutely ruled out that some of the volumetric brain differences between AD, MCI, and normal subjects might arise due to differences in medications, but such effects are likely minimal. The major treatments for AD, including acetylcholine eesterase inhibitors (AChE-I) and NMDA receptor modulators, have effects at the synaptic (neurotransmitter) level that can provide limited symptomatic relief and have not been found to resist the progression of atrophy, despite many efforts to find such effects. In their ADNI study of 269 MCI subjects, Kovacevic et al. (2009) noted that 45% of the MCI subjects were being treated with AchE-Is, but controlling for treatment status in prediction of decline did not change the association between medial temporal lobe volumes on MRI and cognitive decline, not did treatment status affect regional volumes. In addition, some psychiatric medications do have direct effects on brain structure that are not attributable to the illness itself, and these include lithium a treatment for bipolar disorder (Bearden et al., 2007; Bearden et al., 2008), and the antipsychotics haloperidol or olanzapine (Thompson et al., 2009). However, ADNI's exclusion criteria required subjects to be free from major depression, bipolar disorder, or any history of schizophrenia.

## Conclusion

In summary, here we presented a novel method for discovering genetic variations associated with brain structure. The resulting method, termed vGWAS, is capable of integrating a large amount of biological information, yet still allows sufficient power to detect significant variants. This method will be useful in any brain maps that have coordinate systems, such as voxel-based morphometry, cortical surface data, and parameterized tracts derived from diffusion tensor imaging. In addition, we have provided a ranked list of new candidate genes with potential effects on brain structure that are worthy of further study.

## Acknowledgments

## References

Bartholomeusz G, Wu Y, Ali Seyed M, Xia W, Kwong KY, Hortobagyi G, Hung MC. Nuclear translocation of the pro-apoptotic Bcl-2 family member Bok induces apoptosis. Mol.Carcinog 2006;45 (2):73–83. [PubMed: 16302269]

Bearden CE, Thompson PM, Dalwani M, Hayashi KM, Lee AD, Nicoletti M, Trakhtenbroit M, Glahn DC, Brambilla P, Sassi RB, Mallinger AG, Frank E, Kupfer DJ, Soares JC. Greater cortical gray matter

density in lithium-treated patients with bipolar disorder. Biol. Psychiatry 2007;62(1):7–16. [PubMed: 17240360]

Bearden CE, Thompson PM, Dutton RA, Frey BN, Peluso MA, Nicoletti M, Dierschke N, Hayashi KM, Klunder AD, Glahn DC, Brambilla P, Sassi RB, Mallinger AG, Soares JC. Three-dimensional mapping of hippocampal anatomy in unmedicated and lithium-treated patients with bipolar disorder. Neuropsychopharmacology 2008;33(6):1229–1238. [PubMed: 17687266]

Benjamini Y, Hochberg Y. Controlling the false discovery rate—a practical and powerful approach to multiple testing. J. R. Stat Soc, Ser. B Methodol 1995;57(1):289–300.

Benjamini Y, Yekutieli D. The control of the false discovery rate in multiple testing under dependency. Ann. Stat 2001;29(4):1165–1188.

Bingle L, Singleton V, Bingle CD. The putative ovarian tumour marker gene HE4 (WFDC2), is expressed in normal tissues and undergoes complex alternative splicing to yield multiple protein isoforms. Oncogene 2002;21(17):2768–2773. [PubMed: 11965550]

Brun CC, Lepore N, Pennec X, Lee AD, Barysheva M, Madsen SK, Avedissian C, Chou YY, de Zubicaray GI, McMahon KL, Wright MJ, Toga AW, Thompson PM. Mapping the regional influence of genetics on brain structure variability—a tensor-based morphometry study. NeuroImage 2009;48(1):37–49. [PubMed: 19446645]

Brunk I, Blex C, Speidel D, Brose N, Ahnert-Hilger G. Ca2+-dependent activator proteins of secretion promote vesicular monoamine uptake. J. Biol. Chem 2009;284(2):1050–1056. [PubMed: 19008227]

Burges CJC. A tutorial on Support Vector Machines for pattern recognition. Data Mining Knowledge Discov 1998;2(2):121–167.

Chiang MC, Avedissian C, Barysheva M, Toga A, McMahon K, De Zubicaray G, Wright MJ, Thompson P. Extending Genetic Linkage Analysis to Diffusion Tensor Images to Map Single Gene Effects on Brain Fiber Architecture Medical Image Computing and Computer Assisted Intervention. 2009;5762:506–513.

Chou YY, Lepore N, Chiang MC, Avedissian C, Barysheva M, McMahon KL, de Zubicaray GI, Meredith M, Wright MJ, Toga AW, Thompson PM. Mapping genetic influences on ventricular structure in twins. NeuroImage 2009;44(4):1312–1323. [PubMed: 19041405]

Cisternas FA, Vincent JB, Scherer SW, Ray PN. Cloning and characterization of human CADPS and CADPS2, new members of the $Ca^{2+}$-dependent activator for secretion protein family. Genomics 2003;81(3):279–291. [PubMed: 12659812]

Cockrell JR, Folstein MF. Mini-Mental State Examination (MMSE). Psycho-pharmacol. Bull 1988;24 (4):689–692.

Corder EH, Saunders AM, Strittmatter WJ, Schmechel DE, Gaskell PC, Small GW, Roses AD, Haines JL, Pericak-Vance MA. Gene dose of apolipopro-tein E type 4 allele and the risk of Alzheimer's disease in late onset families. Science 1993;261(5123):921–923. [PubMed: 8346443]

Curran-Everett D. Multiple comparisons: philosophies and illustrations. Am. J. Physiol. Regul. Integr. Comp. Physiol 2000;279(1):R1–R8. [PubMed: 10896857]

Dabney AR, Storey JD. A reanalysis of a published Affymetrix GeneChip control dataset. Genome Biol 2006;7(3):401. [PubMed: 16563185]

Dudbridge F, Koeleman BP. Efficient computation of significance levels for multiple associations in large studies of correlated data, including genomewide association studies. Am. J. Hum. Genet 2004;75(3):424–435. [PubMed: 15266393]

Egan MF, Goldberg TE, Kolachana BS, Callicott JH, Mazzanti CM, Straub RE, Goldman D, Weinberger DR. Effect of COMT Val108/158 Met genotype on frontal lobe function and risk for schizophrenia. Proc. Natl. Acad. Sci. U. S. A 2001;98(12):6917–6922. [PubMed: 11381111]

Eran A, Graham KR, Vatalaro K, McCarthy J, Collins C, Peters H, Brewster SJ, Hanson E, Hundley R, Rappaport L, Holm IA, Kohane IS, Kunkel LM. Comment on "Autistic-like phenotypes in Cadps2-knockout mice and aberrant CADPS2 splicing in autistic patients". J. Clin. Invest 2009;119(4):679–680. author reply 680–671. [PubMed: 19339759]

Ewens, WJ.; Grant, GR. 1 ed. New York: Springer; 2001. Statistical Methods in Bioinformatics.

Fillard, P.; Arsigny, V.; Pennec, X.; Thompson, PM.; Ayache, N. 19th International Conference, IPMI 2005. 2005. Extrapolation of sparse tensor fields: application to the modeling of brain variability.

Information Processing in Medical Imaging. Proceedings (Lecture Notes in Computer Science Vol. 3565), 27–38|xxi+777

Frackowiak, RSJ., editor. Human Brain Function. San Diego: Academic Press; 2004.

Frayling TM, Timpson NJ, Weedon MN, Zeggini E, Freathy RM, Lindgren CM, Perry JR, Elliott KS, Lango H, Rayner NW, Shields B, Harries LW, Barrett JC, Ellard S, Groves CJ, Knight B, Patch AM, Ness AR, Ebrahim S, Lawlor DA, Ring SM, Ben-Shlomo Y, Jarvelin MR, Sovio U, Bennett AJ, Melzer D, Ferrucci L, Loos RJ, Barroso I, Wareham NJ, Karpe F, Owen KR, Cardon LR, Walker M, Hitman GA, Palmer CN, Doney AS, Morris AD, Smith GD, Hattersley AT, McCarthy MI. A common variant in the FTO gene is associated with body mass index and predisposes to childhood and adult obesity. Science 2007;316(5826):889–894. [PubMed: 17434869]

Frazer KA, Ballinger DG, Cox DR, Hinds DA, Stuve LL, Gibbs RA, Belmont JW, Boudreau A, Hardenbol P, Leal SM, Pasternak S, Wheeler DA, Willis TD, Yu F, Yang H, Zeng C, Gao Y, Hu H, Hu W, Li C, Lin W, Liu S, Pan H, Tang X, Wang J, Wang W, Yu J, Zhang B, Zhang Q, Zhao H, Zhou J, Gabriel SB, Barry R, Blumenstiel B, Camargo A, Defelice M, Faggart M, Goyette M, Gupta S, Moore J, Nguyen H, Onofrio RC, Parkin M, Roy J, Stahl E, Winchester E, Ziaugra L, Altshuler D, Shen Y, Yao Z, Huang W, Chu X, He Y, Jin L, Liu Y, Sun W, Wang H, Wang Y, Xiong X, Xu L, Waye MM, Tsui SK, Xue H, Wong JT, Galver LM, Fan JB, Gunderson K, Murray SS, Oliphant AR, Chee MS, Montpetit A, Chagnon F, Ferretti V, Leboeuf M, Olivier JF, Phillips MS, Roumy S, Sallee C, Verner A, Hudson TJ, Kwok PY, Cai D, Koboldt DC, Miller RD, Pawlikowska L, Taillon-Miller P, Xiao M, Tsui LC, Mak W, Song YQ, Tam PK, Nakamura Y, Kawaguchi T, Kitamoto T, Morizono T, Nagashima A, Ohnishi Y, Sekine A, Tanaka T, Tsunoda T, Deloukas P, Bird CP, Delgado M, Dermitzakis ET, Gwilliam R, Hunt S, Morrison J, Powell D, Stranger BE, Whittaker P, Bentley DR, Daly MJ, de Bakker PI, Barrett J, Chretien YR, Maller J, McCarroll S, Patterson N, Pe'er I, Price A, Purcell S, Richter DJ, Sabeti P, Saxena R, Schaffner SF, Sham PC, Varilly P, Stein LD, Krishnan L, Smith AV, Tello-Ruiz MK, Thorisson GA, Chakravarti A, Chen PE, Cutler DJ, Kashuk CS, Lin S, Abecasis GR, Guan W, Li Y, Munro HM, Qin ZS, Thomas DJ, McVean G, Auton A, Bottolo L, Cardin N, Eyheramendy S, Freeman C, Marchini J, Myers S, Spencer C, Stephens M, Donnelly P, Cardon LR, Clarke G, Evans DM, Morris AP, Weir BS, Mullikin JC, Sherry ST, Feolo M, Skol A, Zhang H, Matsuda I, Fukushima Y, Macer DR, Suda E, Rotimi CN, Adebamowo CA, Ajayi I, Aniagwu T, Marshall PA, Nkwodimmah C, Royal CD, Leppert MF, Dixon M, Peiffer A, Qiu R, Kent A, Kato K, Niikawa N, Adewole IF, Knoppers BM, Foster MW, Clayton EW, Watkin J, Muzny D, Nazareth L, Sodergren E, Weinstock GM, Yakub I, Birren BW, Wilson RK, Fulton LL, Rogers J, Burton J, Carter NP, Clee CM, Griffiths M, Jones MC, McLay K, Plumb RW, Ross MT, Sims SK, Willey DL, Chen Z, Han H, Kang L, Godbout M, Wallenburg JC, L'Archeveque P, Bellemare G, Saeki K, An D, Fu H, Li Q, Wang Z, Wang R, Holden AL, Brooks LD, McEwen JE, Guyer MS, Wang VO, Peterson JL, Shi M, Spiegel J, Sung LM, Zacharia LF, Collins FS, Kennedy K, Jamieson R, Stewart J. A second generation human haplotype map of over 3.1 million SNPs. Nature 2007;449(7164):851–861. [PubMed: 17943122]

Freund Y, Schapire RE. A decision-theoretic generalization of on-line learning and an application to boosting. J. Comput. Sys. Sci 1997;55(1):119–139.

Friston KJ, Holmes AP, Worsley KJ, Poline J-P, Frith CD, Frackowiak RSJ. Statistical parametric maps in functional imaging: a general linear approach. Hum. Brain Mapp 1994;2(4):189–210.

Frisoni GB, Fox NC, Jack CR, Scheltens P, Thompson PM. The Clinical Use of Structural MRI in Alzheimer's Disease. Nat Rev Neurol. in press.

Gao X, Starmer J, Martin ER. A multiple testing correction method for genetic association studies using correlated single nucleotide polymorphisms. Genet. Epidemiol 2008;32(4):361–369. [PubMed: 18271029]

Gao X, Becker LC, Becker DM, Starmer JD, Province MA. Avoiding the high Bonferroni penalty in genome-wide association studies. Genet. Epidemiol 2010;34(1):100–105. [PubMed: 19434714]

Genovese CR, Lazar NA, Nichols T. Thresholding of statistical maps in functional neuroimaging using the false discovery rate. NeuroImage 2002;15(4):870–878. [PubMed: 11906227]

Glahn DC, Paus T, Thompson PM. Imaging genomics: mapping the influence of genetics on brain structure and function. Hum. Brain Mapp 2007a;28(6):461–463. [PubMed: 17471577]

Glahn DC, Thompson PM, Blangero J. Neuroimaging endophenotypes: strategies for finding genes influencing brain structure and function. Hum. Brain Mapp 2007b;28(6):488–501. [PubMed: 17440953]

Gottesman II, Gould TD. The endophenotype concept in psychiatry: etymology and strategic intentions. Am. J. Psychiatry 2003;160(4):636–645. [PubMed: 12668349]

Grenander U, Miller MI. Computational anatomy: an emerging discipline. Q. Appl. Math 1998;56(4): 617–694.

Gu X, Frankowski RF, Rosner GL, Relling M, Peng B, Amos CI. A modified forward multiple regression in high-density genome-wide association studies for complex traits. Genet. Epidemiol 2009;33(6): 518–525. [PubMed: 19365845]

Hayasaka, S. Fifth International Imaging Genetics Conference. Irvine, CA: University of California, Irvine; 2009. Power in Whole-Brain Whole-Genome Association Studies.

Ho, AJ.; Hua, X.; Lee, S.; Leow, AD.; Yanovsky, I.; Gutman, B.; Dinov, I.; Lepore, N.; Stein, JL.; Toga, A.; Jack, C.; Bernstein, MA.; Reiman, EM.; Harvey, D.; Kornak, J.; Schuff, N.; Alexander, G.; Weiner, M.; Thompson, P. Hum Brain Mapp. Comparing 3 Tesla and 1.5 Tesla MRI for tracking Alzheimer's disease progression with tensor-based morphometry. in press

Ho AJ, Stein JL, Hua X, Lee S, Hibar DP, Leow AD, Dinov ID, Toga A, Saykin AJ, Shen L, Foroud T, Pankratz N, Huentelman MJ, Craig DW, Gerber JD, Allen A, Corneveaux J, Stephan DA, Webster J, DeChairo BM, Potkin SG, Jack C, Weiner M, Raji CA, Lopez OL, Becker JT, Thompson PT. A commonly carried allele of the obesity-related FTO gene is associated with reduced brain volume in healthy elderly. submitted for publication.

Hoenig JM, Heisey DM. The abuse of power: the pervasive fallacy of power calculations for data analysis. Am. Stat 2001;55(1):19–24.

Hotelling H. The most predictable criterion. J. Educ. Psychol 1935;26:139–142.

Hotelling H. Relations between two sets of variates. Biometrika 1936;28:321–377.

Hua X, Leow AD, Parikshak N, Lee S, Chiang MC, Toga AW, Jack CR Jr, Weiner MW, Thompson PM. Tensor-based morphometry as a neuroimaging biomarker for Alzheimer's disease: an MRI study of 676 AD, MCI, and normal subjects. NeuroImage 2008;43(3):458–469. [PubMed: 18691658]

Hua X, Lee S, Yanovsky I, Leow AD, Chou YY, Ho AJ, Gutman B, Toga AW, Jack CR Jr, Bernstein MA, Reiman EM, Harvey D, Kornak J, Schuff N, Alexander GE, Weiner MW, Thompson PM. Optimizing power to track brain degeneration in Alzheimer's disease and mild cognitive impairment with tensor-based morphometry: an ADNI study of 515 subjects. NeuroImage 2009;48(4):668–671. [PubMed: 19615450]

Hulshoff Pol HE, Schnack HG, Posthuma D, Mandl RC, Baare WF, van Oel C, van Haren NE, Collins DL, Evans AC, Amunts K, Burgel U, Zilles K, de Geus E, Boomsma DI, Kahn RS. Genetic contributions to human brain morphology and intelligence. J. Neurosci 2006;26(40):10235–10242. [PubMed: 17021179]

Jack CR Jr, Bernstein MA, Fox NC, Thompson P, Alexander G, Harvey D, Borowski B, Britson PJL, Whitwell J, Ward C, Dale AM, Felmlee JP, Gunter JL, Hill DL, Killiany R, Schuff N, Fox-Bosetti S, Lin C, Studholme C, DeCarli CS, Krueger G, Ward HA, Metzger GJ, Scott KT, Mallozzi R, Blezek D, Levy J, Debbins JP, Fleisher AS, Albert M, Green R, Bartzokis G, Glover G, Mugler J, Weiner MW. The Alzheimer's Disease Neuroimaging Initiative (ADNI): MRI methods. J. Magn. Reson. Imaging 2008;27(4):685–691. [PubMed: 18302232]

Kent WJ, Sugnet CW, Furey TS, Roskin KM, Pringle TH, Zahler AM, Haussler D. The human genome browser at UCSC. Genome Res 2002;12(6):996–1006. [PubMed: 12045153]

Kovacevic S, Rafii MS, Brewer JB. High-throughput, fully automated volumetry for prediction of MMSE and CDR decline in mild cognitive impairment. Alzheimer Dis. Assoc. Disord 2009;23(2):139–145. [PubMed: 19474571]

Lahiri DK, Bye S, Nurnberger JI Jr, Hodes ME, Crisp M. A non-organic and non-enzymatic extraction method gives higher yields of genomic DNA from whole-blood samples than do nine other methods tested. J. Biochem. Biophys. Methods 1992;25(4):193–205. [PubMed: 1494032]

Lander ES, Schork NJ. Genetic dissection of complex traits. Science 1994;265(5181):2037–2048. [PubMed: 8091226]

Lau WL, Scholnick SB. Identification of two new members of the CSMD gene family. Genomics 2003;82 (3):412–415. [PubMed: 12906867]

Lee, AD.; Lepore, N.; Barysheva, M.; Chou, YY.; Schwartzman, A.; Brun, CC.; Madsen, S.; McMahon, K.; De Zubicaray, G.; Wright, MJ.; Martin, NG.; Toga, A.; Thompson, P. A Multivariate analysis of the Effects of Genes and Environment on Brain Fiber Architecture. submitted for publication

Leek JT, Storey JD. A general framework for multiple testing dependence. Proc. Natl. Acad. Sci. U. S. A 2008;105(48):18718–18723. [PubMed: 19033188]

Leow A, Huang SC, Geng A, Becker J, Davis S, Toga A, Thompson P. Inverse consistent mapping in 3D deformable image registration: its construction and statistical properties. Inf. Process Med. Imaging 2005;19:493–503. [PubMed: 17354720]

Lesch KP, Timmesfeld N, Renner TJ, Halperin R, Roser C, Nguyen TT, Craig DW, Romanos J, Heine M, Meyer J, Freitag C, Warnke A, Romanos M, Schafer H, Walitza S, Reif A, Stephan DA, Jacob C. Molecular genetics of adult ADHD: converging evidence from genome-wide association and extended pedigree linkage studies. J. Neural. Transm 2008;115(11):1573–1585. [PubMed: 18839057]

Levine, M.; Ensom, MHH. Pharmacotherapy. Vol. 21. 2001. Post hoc power analysis: an idea whose time has passed?; p. 405-409.

Li J, Ji L. Adjusting multiple testing in multilocus analyses using the eigenvalues of a correlation matrix. Heredity 2005;95(3):221–227. [PubMed: 16077740]

Li Y, Willer C, Sanna S, Abecasis G. Genotype imputation. Annu. Rev. Genomics Hum. Genet 2009;10:387–406. [PubMed: 19715440]

Lindholm CK. IL-2 receptor signaling through the Shb adapter protein in T and NK cells. Biochem. Biophys. Res. Commun 2002;296(4):929–936. [PubMed: 12200137]

Liu QR, Drgon T, Johnson C, Walther D, Hess J, Uhl GR. Addiction molecular genetics: 639,401 SNP whole genome association identifies many "cell adhesion" genes. Am. J. Med. Genet. B Neuropsychiatr. Genet 2006;141B(8):918–925. [PubMed: 17099884]

Liu J, Pearlson G, Windemuth A, Ruano G, Perrone-Bizzozero NI, Calhoun V. Combining fMRI and SNP data to investigate connections between brain function and genetics using parallel ICA. Hum. Brain Mapp 2009;30(1):241–255. [PubMed: 18072279]

Lo KY, Li Z, Wang F, Marcotte EM, Johnson AW. Ribosome stalk assembly requires the dual-specificity phosphatase Yvh1 for the exchange of Mrt4 with P0. J. Cell Biol 2009;186(6):849–862. [PubMed: 19797078]

Lundwall A. A locus on chromosome 20 encompassing genes that are highly expressed in the epididymis. Asian J. Androl 2007;9(4):540–544. [PubMed: 17589793]

Mazziotta J, Toga A, Evans A, Fox P, Lancaster J, Zilles K, Woods R, Paus T, Simpson G, Pike B, Holmes C, Collins L, Thompson P, MacDonald D, Iacoboni M, Schormann T, Amunts K, Palomero-Gallagher N, Geyer S, Parsons L, Narr K, Kabani N, Le Goualher G, Boomsma D, Cannon T, Kawashima R, Mazoyer B. A probabilistic atlas and reference system for the human brain: International Consortium for Brain Mapping (ICBM). Philos. Trans. R. Soc. Lond. B Biol. Sci 2001;356(1412):1293–1322. [PubMed: 11545704]

McCarthy MI, Abecasis GR, Cardon LR, Goldstein DB, Little J, Ioannidis JP, Hirschhorn JN. Genome-wide association studies for complex traits: consensus, uncertainty and challenges. Nat. Rev., Genet 2008;9(5):356–369. [PubMed: 18398418]

McKhann G, Drachman D, Folstein M, Katzman R, Price D, Stadlan EM. Clinical diagnosis of Alzheimer's disease: report of the NINCDS-ADRDA Work Group under the auspices of Department of Health and Human Services Task Force on Alzheimer's Disease. Neurology 1984;34(7):939–944. [PubMed: 6610841]

Meyer-Lindenberg A, Weinberger DR. Intermediate phenotypes and genetic mechanisms of psychiatric disorders. Nat. Rev., Neurosci 2006;7(10):818–827. [PubMed: 16988657]

Mindnich RD, Penning TM. Aldo-keto reductase (AKR) superfamily: genomics and annotation. Hum. Genomics 2009;3(4):362–370. [PubMed: 19706366]

Morra JH, Tu Z, Apostolova LG, Green AE, Avedissian C, Madsen SK, Parikshak N, Hua X, Toga AW, Jack CR Jr, Weiner MW, Thompson PM. Validation of a fully automated 3D hippocampal

segmentation method using subjects with Alzheimer's disease mild cognitive impairment, and elderly controls. NeuroImage 2008;43(1):59–68. [PubMed: 18675918]

Morra, JH.; Tu, Z.; Toga, A.; Thompson, P. Machine learning for brain image segmentation. In: Gonzalez, F.; Romero, E., editors. Biomedical Image Analysis and Machine Learning Technologies. 2009.

Morris JC. The Clinical Dementia Rating (CDR): current version and scoring rules. Neurology 1993;43 (11):2412–2414. [PubMed: 8232972]

Mueller SG, Weiner MW, Thal LJ, Petersen RC, Jack C, Jagust W, Trojanowski JQ, Toga AW, Beckett L. The Alzheimer's disease neuroimaging initiative. Neuroimaging Clin. N. Am 2005;15(4):869–877. xi-xii. [PubMed: 16443497]

Neitzel H. A routine method for the establishment of permanent growing lymphoblastoid cell lines. Hum. Genet 1986;73(4):320–326. [PubMed: 3017841]

Nichols T, Hayasaka S. Controlling the familywise error rate in functional neuroimaging: a comparative review. Stat. Methods Med. Res 2003;12(5):419–446. [PubMed: 14599004]

Panizzon MS, Fennema-Notestine C, Eyler LT, Jernigan TL, Prom-Wormley E, Neale M, Jacobson K, Lyons MJ, Grant MD, Franz CE, Xian H, Tsuang M, Fischl B, Seidman L, Dale A, Kremen WS. Distinct genetic influences on cortical surface area and cortical thickness. Cereb. Cortex 2009;19 (11):2728–2735. [PubMed: 19299253]

Peper JS, Brouwer RM, Boomsma DI, Kahn RS, Hulshoff Pol HE. Genetic influences on human brain structure: a review of brain imaging studies in twins. Hum. Brain Mapp 2007;28(6):464–473. [PubMed: 17415783]

Petersen RC. Aging, mild cognitive impairment, and Alzheimer's disease. Neurol. Clin 2000;18(4):789–806. [PubMed: 11072261]

Pezawas L, Verchinski BA, Mattay VS, Callicott JH, Kolachana BS, Straub RE, Egan MF, Meyer-Lindenberg A, Weinberger DR. The brain-derived neurotrophic factor val66met polymorphism and variation in human cortical morphology. J. Neurosci 2004;24(45):10099–10102. [PubMed: 15537879]

Posthuma D, De Geus EJ, Baare WF, Hulshoff Pol HE, Kahn RS, Boomsma DI. The association between brain volume and intelligence is of genetic origin. Nat. Neurosci 2002;5(2):83–84. [PubMed: 11818967]

Potkin SG, Guffanti G, Lakatos A, Turner JA, Kruggel F, Fallon JH, Saykin AJ, Orro A, Lupoli S, Salvi E, Weiner M, Macciardi F. Hippocampal atrophy as a quantitative trait in a genome-wide association study identifying novel susceptibility genes for Alzheimer's disease. PLoS One 4 2009a;8:e6501.

Potkin SG, Turner JA, Guffanti G, Lakatos A, Fallon JH, Nguyen DD, Mathalon D, Ford J, Lauriello J, Macciardi F. A genome-wide association study of schizophrenia using brain activation as a quantitative phenotype. Schizophr. Bull 2009b;35(1):96–108. [PubMed: 19023125]

Pounds SB. Estimation and control of multiple testing error rates for microarray studies. Brief Bioinform 2006;7(1):25–36. [PubMed: 16761362]

Purcell S, Neale B, Todd-Brown K, Thomas L, Ferreira MA, Bender D, Maller J, Sklar P, de Bakker PI, Daly MJ, Sham PC. PLINK: a tool set for whole-genome association and population-based linkage analyses. Am. J. Hum. Genet 2007;81(3):559–575. [PubMed: 17701901]

Purcell SM, Wray NR, Stone JL, Visscher PM, O'Donovan MC, Sullivan PF, Sklar P. Common polygenic variation contributes to risk of schizophrenia and bipolar disorder. Nature 2009;460(7256):748–752. [PubMed: 19571811]

Roussigne M, Kossida S, Lavigne AC, Clouaire T, Ecochard V, Glories A, Amalric F, Girard JP. The THAP domain: a novel protein motif with similarity to the DNA-binding domain of P element transposase. Trends Biochem. Sci 2003;28(2):66–69. [PubMed: 12575992]

Sabatti C, Service SK, Hartikainen AL, Pouta A, Ripatti S, Brodsky J, Jones CG, Zaitlen NA, Varilo T, Kaakinen M, Sovio U, Ruokonen A, Laitinen J, Jakkula E, Coin L, Hoggart C, Collins A, Turunen H, Gabriel S, Elliot P, McCarthy MI, Daly MJ, Jarvelin MR, Freimer NB, Peltonen L. Genome-wide association analysis of metabolic traits in a birth cohort from a founder population. Nat. Genet 2009;41(1):35–46. [PubMed: 19060910]

Sadakata T, Washida M, Iwayama Y, Shoji S, Sato Y, Ohkura T, Katoh-Semba R, Nakajima M, Sekine Y, Tanaka M, Nakamura K, Iwata Y, Tsuchiya KJ, Mori N, Detera-Wadleigh SD, Ichikawa H, Itohara

S, Yoshikawa T, Furuichi T. Autistic-like phenotypes in Cadps2-knockout mice and aberrant CADPS2 splicing in autistic patients. J. Clin. Invest 2007;117(4):931–943. [PubMed: 17380209]

Sakai Y, Saijo M, Coelho K, Kishino T, Niikawa N, Taya Y. cDNA sequence and chromosomal localization of a novel human protein, RBQ-1 (RBBP6), that binds to the retinoblastoma gene product. Genomics 1995;30(1):98–101. [PubMed: 8595913]

Schmitt JE, Eyler LT, Giedd JN, Kremen WS, Kendler KS, Neale MC. Review of twin and family studies on neuroanatomic phenotypes and typical neurodevelopment. Twin Res. Hum. Genet 2007;10(5): 683–694. [PubMed: 17903108]

Schmitt JE, Lenroot RK, Wallace GL, Ordaz S, Taylor KN, Kabani N, Greenstein D, Lerch JP, Kendler KS, Neale MC, Giedd JN. Identification of genetically mediated cortical networks: a multivariate study of pediatric twins and siblings. Cereb. Cortex 2008;18(8):1737–1747.

Seshadri, S.; DeStefano, AL.; Au, R.; Massaro, JM.; Beiser, AS.; Kelly-Hayes, M.; Kase, CS.; D'Agostino, RB., Sr; Decarli, C.; Atwood, LD.; Wolf, PA. BMC Med. Genet. Vol. 8. 2007. Genetic correlates of brain aging on MRI and cognitive test measures: a genome-wide association and linkage analysis in the Framingham Study; p. pS15

Skol AD, Scott LJ, Abecasis GR, Boehnke M. Joint analysis is more efficient than replication-based analysis for two-stage genome-wide association studies. Nat. Genet 2006;38(2):209–213. [PubMed: 16415888]

Speidel D, Varoqueaux F, Enk C, Nojiri M, Grishanin RN, Martin TF, Hofmann K, Brose N, Reim K. A family of Ca2+-dependent activator proteins for secretion: comparative analysis of structure, expression, localization, and function. J. Biol. Chem 2003;278(52):52802–52809. [PubMed: 14530279]

Stein JL, Hua X, Morra JH, Lee S, Ho AJ, Leow AD, Toga A, Sul J, Kang HM, Eskin E, Saykin AJ, Shen L, Foroud T, Pankratz N, Huentelman MJ, Craig DW, Gerber JD, Allen A, Corneveaux J, Stephan DA, Webster J, DeChairo BM, Potkin SG, Jack C, Weiner M, Thompson P. Genome-Wide Analysis Reveals Novel Genes Influencing Temporal Lobe Structure with Relevance to Neurodegeneration in Alzheimer's Disease. submitted for publication.

Storey JD. The positive false discovery rate: a Bayesian interpretation and the q-value. Ann. Stat 2003;31 (6):2013–2035.

Storey JD, Tibshirani R. Statistical significance for genomewide studies. Proc. Natl. Acad. Sci. U. S. A 2003;100(16):9440–9445. [PubMed: 12883005]

Strausberg RL, Feingold EA, Grouse LH, Derge JG, Klausner RD, Collins FS, Wagner L, Shenmen CM, Schuler GD, Altschul SF, Zeeberg B, Buetow KH, Schaefer CF, Bhat NK, Hopkins RF, Jordan H, Moore T, Max SI, Wang J, Hsieh F, Diatchenko L, Marusina K, Farmer AA, Rubin GM, Hong L, Stapleton M, Soares MB, Bonaldo MF, Casavant TL, Scheetz TE, Brownstein MJ, Usdin TB, Toshiyuki S, Carninci P, Prange C, Raha SS, Loquellano NA, Peters GJ, Abramson RD, Mullahy SJ, Bosak SA, McEwan PJ, McKernan KJ, Malek JA, Gunaratne PH, Richards S, Worley KC, Hale S, Garcia AM, Gay LJ, Hulyk SW, Villalon DK, Muzny DM, Sodergren EJ, Lu X, Gibbs RA, Fahey J, Helton E, Ketteman M, Madan A, Rodrigues S, Sanchez A, Whiting M, Young AC, Shevchenko Y, Bouffard GG, Blakesley RW, Touchman JW, Green ED, Dickson MC, Rodriguez AC, Grimwood J, Schmutz J, Myers RM, Butterfield YS, Krzywinski MI, Skalska U, Smailus DE, Schnerch A, Schein JE, Jones SJ, Marra MA. Generation and initial analysis of more than 15,000 full-length human and mouse cDNA sequences. Proc. Natl. Acad. Sci. U. S. A 2002;99(26):16899–16903. [PubMed: 12477932]

Styner M, Lieberman JA, McClure RK, Weinberger DR, Jones DW, Gerig G. Morphometric analysis of lateral ventricles in schizophrenia and healthy controls regarding genetic and disease-specific factors. Proc. Natl. Acad. Sci. U. S. A 2005;102(13):4872–4877. [PubMed: 15772166]

Sun D, van Erp TG, Thompson PM, Bearden CE, Daley M, Kushan L, Hardt ME, Nuechterlein KH, Toga AW, Cannon TD. Elucidating a magnetic resonance imaging-based neuroanatomic biomarker for psychosis: classification analysis using probabilistic brain atlas and machine learning algorithms. Biol. Psychiatry 2009;66(11):1055–1060. [PubMed: 19729150]

Thompson, PM.; Martin, NG. The ENIGMA Network. 2010. URL: http://enigma.loni.ucla.edu

Thompson PM, Cannon TD, Narr KL, van Erp T, Poutanen VP, Huttunen M, Lonnqvist J, Standertskjold-Nordenstam CG, Kaprio J, Khaledy M, Dail R, Zoumalan CI, Toga AW. Genetic influences on brain structure. Nat. Neurosci 2001;4(12):1253–1258. [PubMed: 11694885]

Thompson PM, Bartzokis G, Hayashi KM, Klunder AD, Lu PH, Edwards N, Hong MS, Yu M, Geaga JA, Toga AW, Charles C, Perkins DO, McEvoy J, Hamer RM, Tohen M, Tollefson GD, Lieberman JA. Time-lapse mapping of cortical changes in schizophrenia with different treatments. Cereb. Cortex 2009;19(5):1107–1123. [PubMed: 18842668]

Toga AW. Neuroimage databases: the good, the bad and the ugly. Nat. Rev., Neurosci 2002;3(4):302–309. [PubMed: 11967560]

Wellcome Trust Case Control Consortium. Genome-wide association study of 14,000 cases of seven common diseases and 3,000 shared controls. Nature 2007;447(7145):661–678. [PubMed: 17554300]

Yanovsky I, Leow AD, Lee S, Osher SJ, Thompson PM. Comparing registration methods for mapping brain change using tensor-based morphometry. Med. Image Anal 2009;13(5):679–700. [PubMed: 19631572]

Zhang Y, Zhu W, Wang YG, Liu XJ, Jiao L, Liu X, Zhang ZH, Lu CL, He C. Interaction of SH2-Bbeta with RET is involved in signaling of GDNF-induced neurite outgrowth. J. Cell Sci 2006;119(Pt. 8):1666–1676. [PubMed: 16569669]

Zhuang B, Su YS, Sockanathan S. FARP1 promotes the dendritic growth of spinal motor neuron subtypes through transmembrane Semaphorin6A and PlexinA4 signaling. Neuron 2009;61(3):359–372. [PubMed: 19217374]
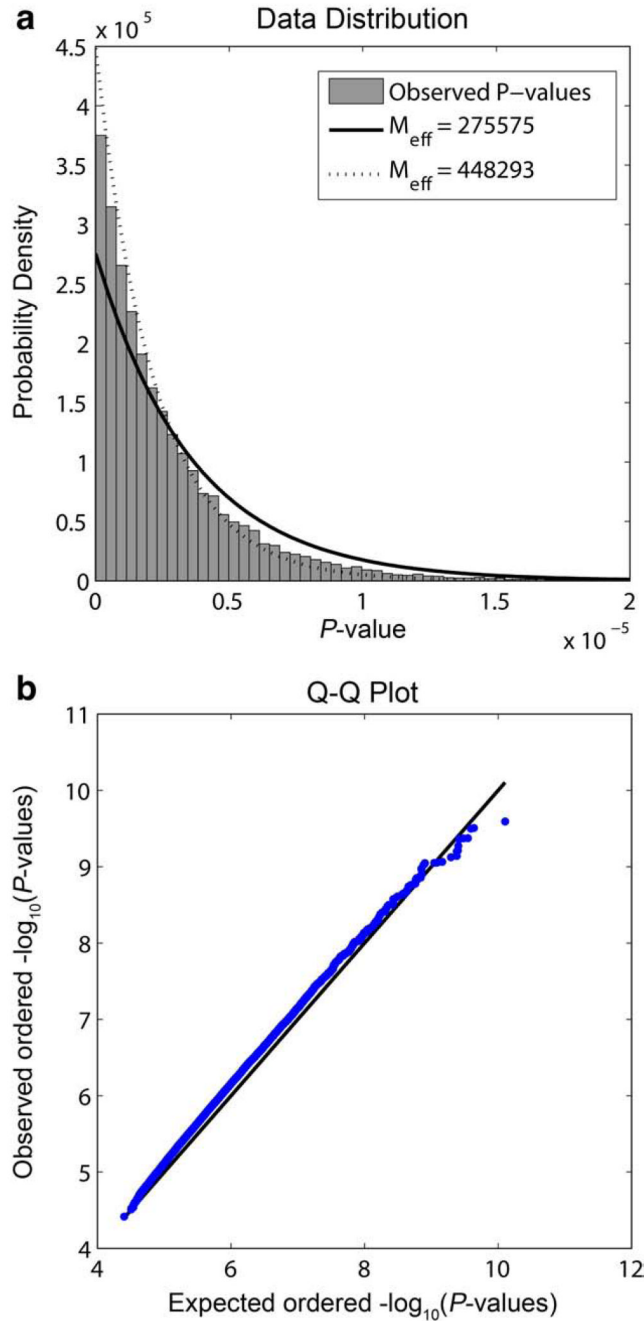
**Fig. 1.**
The theoretical and observed distributions of the minimum *P*-value across voxels. (a) The normalized histogram of the observed minimum *P*-values is shown. Lines represent the PDF of the *Beta*(1, 275575) distribution (solid line) based on $M_{\text{eff}}$ and the *Beta*(1, 448293) distribution (dashed line) based on the number of measured markers. (b) The Q–Q plot shows the observed *P*-values plotted against those expected from the *Beta*(1, 275575) (blue dots). The black line gives a purely null distribution. The observed data matches well with that expected by the $M_{\text{eff}}$ based null distribution. (For interpretation of the references to colour in this figure legend, the reader is referred to the web version of this article.)
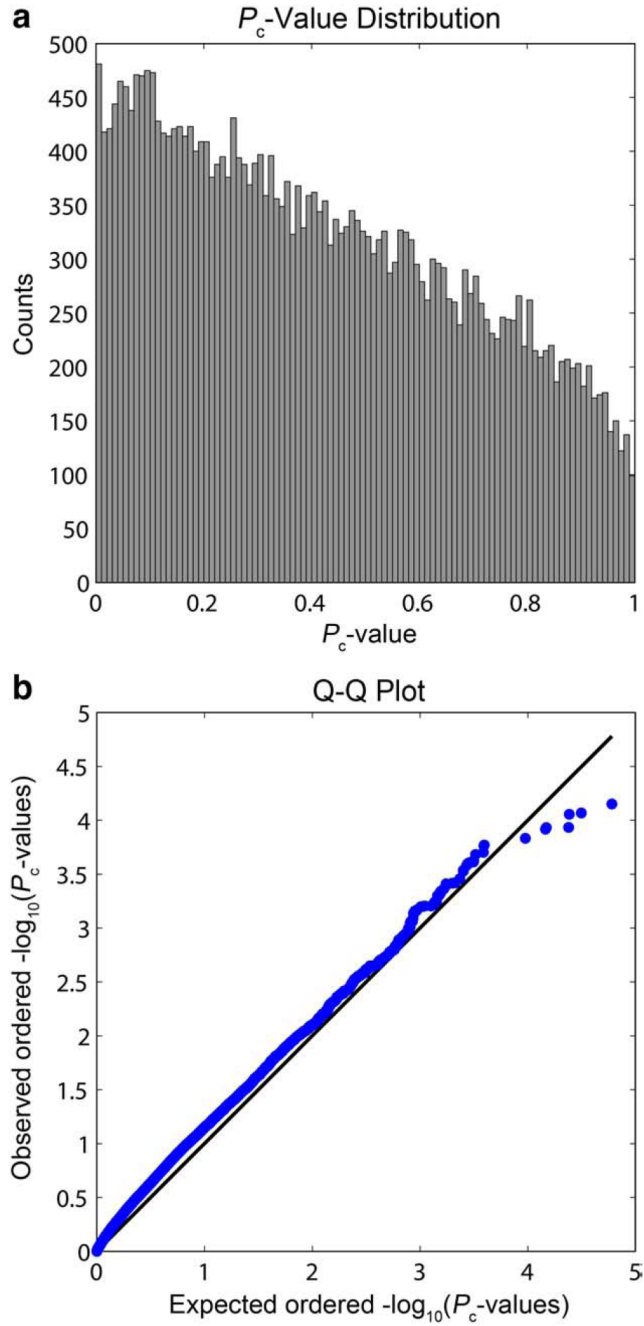
**Fig. 2.**
A histogram and quantile–quantile plot for the "corrected" $P$-values ($P_c$-values). (a) The histogram shows the $P_c$-values approximately follow a uniform distribution. (b) The Q–Q plot shows the expected ordered $-\log_{10}(P_c\text{-values})$ as drawn from a uniform distribution plotted against the observed ordered $-\log_{10}(P_c\text{-values})$ as blue dots. The black line shows the null distribution. (For interpretation of the references to colour in this figure legend, the reader is referred to the web version of this article.)
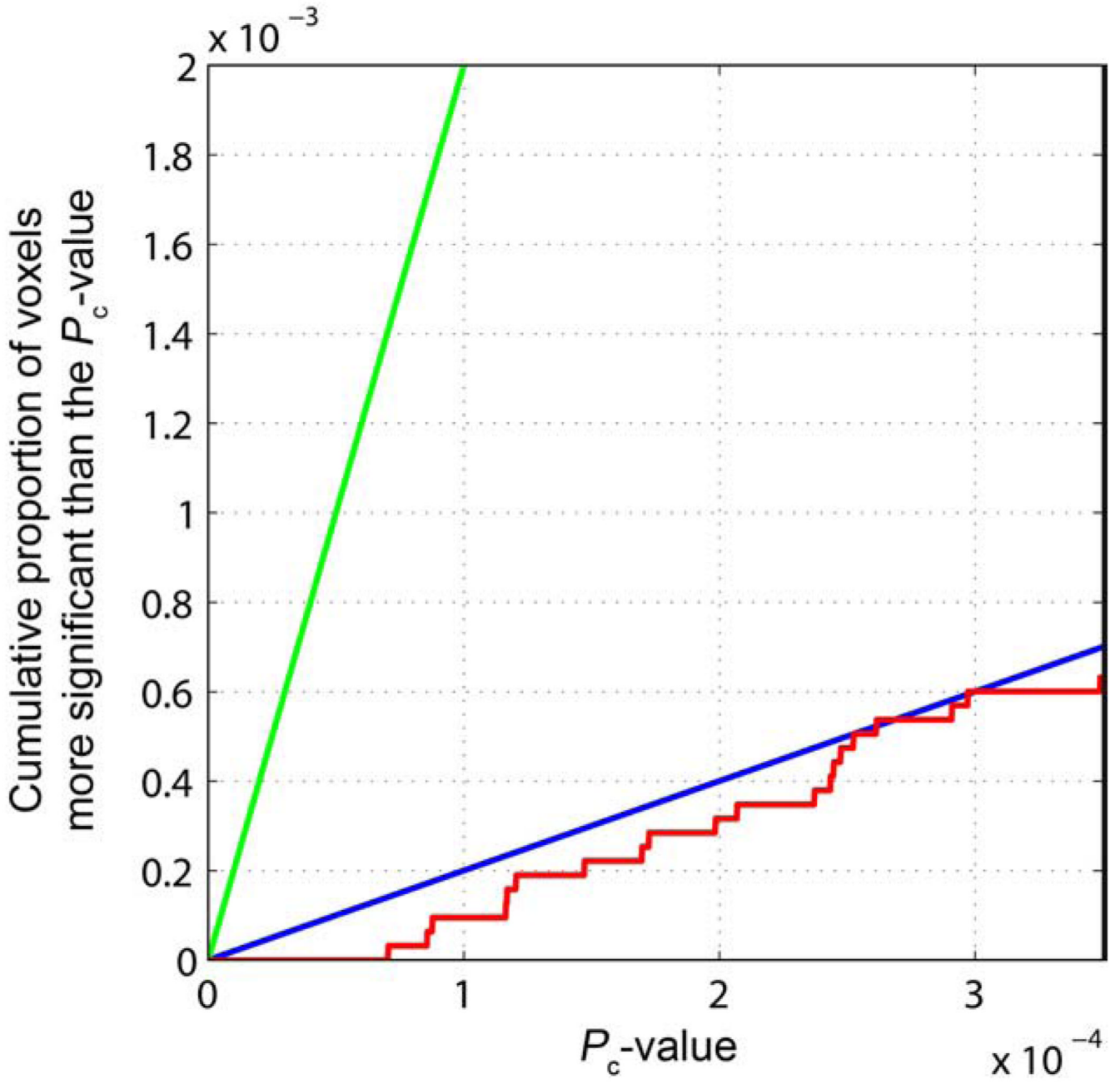
**Fig. 3.**
The cumulative distribution function of corrected *P*-values. The cumulative distribution function of $P_c$-values is shown (red) with two lines representing thresholds of $q$=0.50 (blue), and $q$=0.05 (green). (For interpretation of the references to colour in this figure legend, the reader is referred to the web version of this article.)
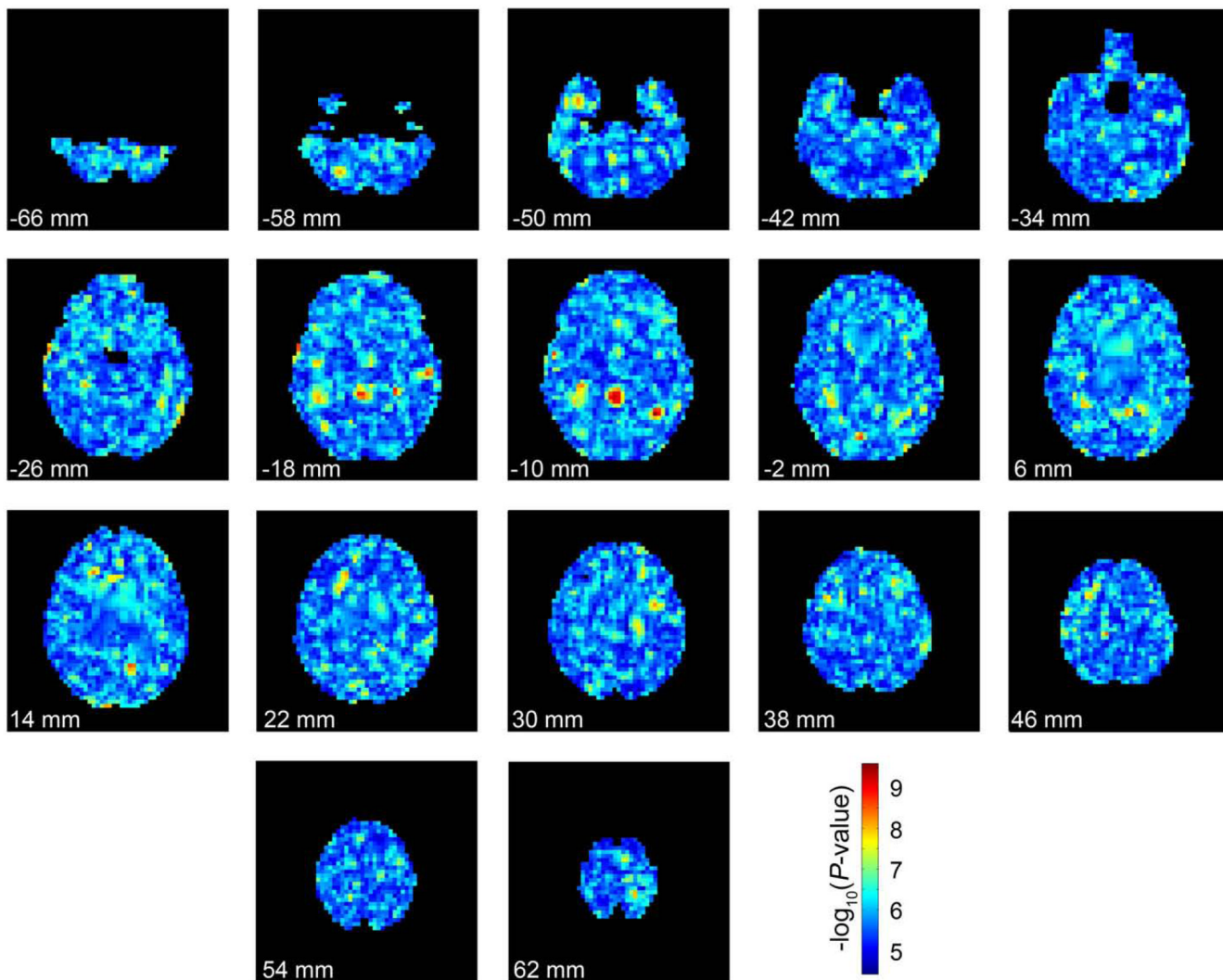
**Fig. 4.**
The significance of the most associated SNP at each voxel. Each image represents slices through the brain at 8 mm intervals from inferior to superior. The top of the page represents anterior of the brain and the bottom of represents posterior. The images are in radiological convention (left of the image is the right side of the subject). Each voxel is colored by the −$\log_{10}$ of the *P*-value of the genetic association at each point (warmer colors are more strongly associated). (For interpretation of the references to colour in this figure legend, the reader is referred to the web version of this article.)
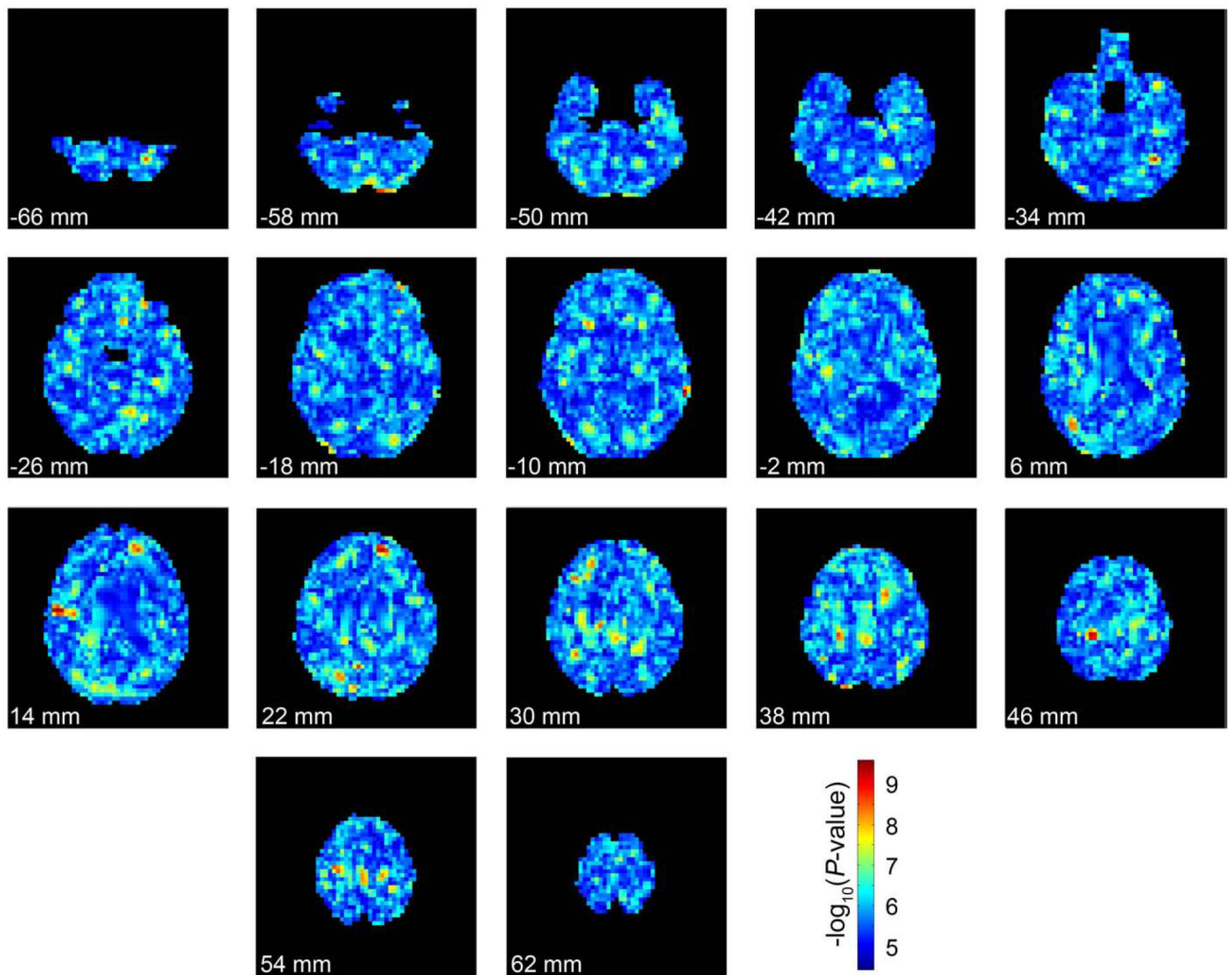
**Fig. 5.**
The significance of the most strongly associated SNP at each voxel in a single permuted dataset. Each image represents slices through the brain at 8 mm intervals from inferior to superior. The top of the page represents anterior of the brain and the bottom of represents posterior. The images are in radiological convention (left of the image is the right side of the subject). Each voxel is colored by the $-\log_{10}$ of the $P$-value of the genetic association at each point (warmer colors are more strongly associated). The same color scale is used from Fig. 4 for comparisons. (For interpretation of the references to colour in this figure legend, the reader is referred to the web version of this article.)
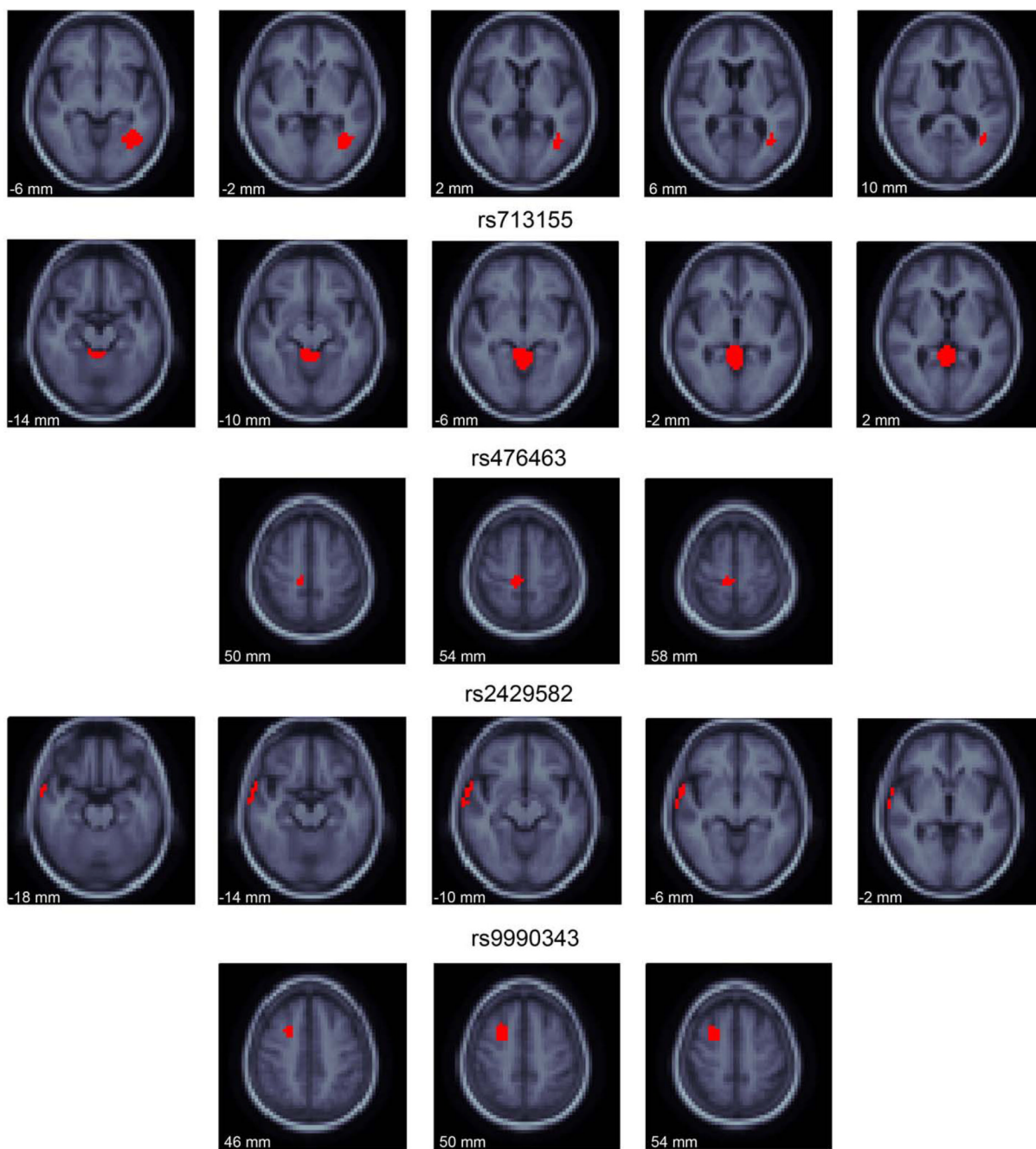
**Fig. 6.**
The locations of association for the 5 most associated SNPs. Slices through the MDT are shown in regions where the indicated SNP is the most associated at the voxel (red). The SNPs have effects on brain structure beyond the red colored voxels, but these voxels are associated with the labeled SNP more than any other. The slices through the MDT are every 4 mm and go from inferior (left of page) to superior (right of page). The images are in radiological convention (left of the image is the right side of the subject). (For interpretation of the references to colour in this figure legend, the reader is referred to the web version of this article.)
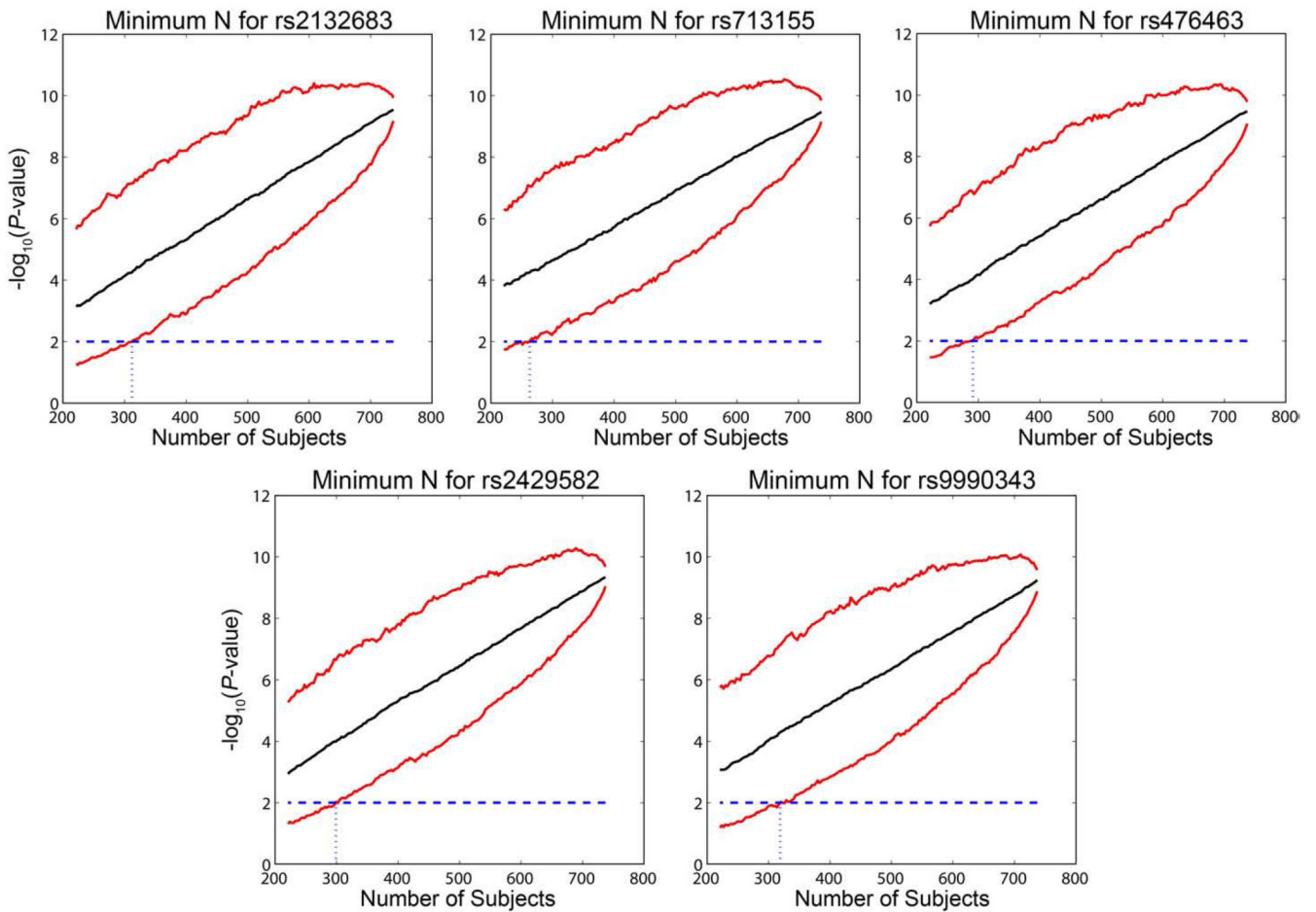
**Fig. 7.**
The minimum number of subjects needed to replicate the findings for the top 5 most associated
SNPs was estimated with a resampling approach. Subjects were randomly removed from each
of the diagnostic categories until none was left in a category, and the association P-value of
the SNP was calculated. This process was repeated 1000 times, to estimate 95% confidence
intervals (red lines). The median *P*-value of the repetitions for each number of subjects removed
is shown as the solid black line. The blue line shows the replication threshold for the first 5
SNPs, a Bonferroni corrected *P*-value of 0.01. The dotted blue line shows the estimated
minimum sample size that would be required to detect a replication of the finding with 95%
confidence (*N*=312 for rs2132683; *N*=263 for rs713155; N=291 for rs476463; N=299 for
rs2429582; *N*=319 for rs9990343). (For interpretation of the references to colour in this figure
legend, the reader is referred to the web version of this article.)

**Table 1**

Number of SNPs measured and the effective number of tests ($M_{\text{eff}}$) on each chromosome. The effective number of tests was not estimated in sex chromosomes or for mitochondrial DNA, where the effective number of tests was set to be equal to the number of SNPs measured in those regions, rather than a smaller number. This is the most conservative estimate. Chromosome XY refers to SNPs on both the X and Y chromosomes.

| Chr | Number of SNPs | $M_{\text{eff}}$ |
|---|---|---|
| 1 | 33,850 | 20,205 |
| 2 | 36,384 | 21,747 |
| 3 | 30,765 | 18,275 |
| 4 | 27,072 | 15,972 |
| 5 | 27,396 | 16,245 |
| 6 | 30,054 | 16,669 |
| 7 | 24,446 | 14,680 |
| 8 | 24,768 | 14,710 |
| 9 | 21,283 | 13,231 |
| 10 | 23,089 | 13,806 |
| 11 | 21,796 | 13,066 |
| 12 | 21,461 | 12,787 |
| 13 | 16,605 | 9809 |
| 14 | 14,501 | 8916 |
| 15 | 13,355 | 8557 |
| 16 | 13,460 | 9111 |
| 17 | 11,721 | 7764 |
| 18 | 13,198 | 8232 |
| 19 | 7,895 | 5425 |
| 20 | 11,169 | 7148 |
| 21 | 6,582 | 4193 |
| 22 | 6,757 | 4341 |
| X | 10,637 | 10,637 |
| Y | 12 | 12 |
| XY | 25 | 25 |
| Mitochondrial | 12 | 12 |
| Total | 448,293 | 275,575 |

**Table 2**

The top 20 most associated SNPs organized by minimum $P$-value at any voxel. The identifier of each SNP is shown with its minor allele frequency (MAF), and the number of subjects in each genotype group (homozygous major allele, Maj; heterozygous, Het; homozygous minor allele, Min). Note that the number of subjects in each genotype group may not add up to the total number of subjects (740) if data is missing for that SNP in some subjects. The volume of all the voxels where this SNP was the most associated SNP is shown in the Volume (mm$^3$) column. Minimum $P$-value gives the raw $P$-value at the most associated voxel where this SNP was a winner. Mean $P$-value gives the mean $P$-value of association across all voxels where it is the winning SNP. Additionally, the gene or expressed sequence tag (EST) within 50 kb is shown, where bold typeface indicates that the SNP is located in the gene or EST.

| Chr | Base Pair | SNP | MAF | Number of subjects in genotype groups | | | Volume (mm$^3$) | Minimum $P$-value | Mean $P$-value | Gene or EST (± 50 kb) |
|---|---|---|---|---|---|---|---|---|---|---|
| | | | | Maj | Het | Min | | | | |
| 6q16.2 | 99778735 | rs2132683 | 0.3257 | 340 | 318 | 82 | 4224 | $2.56\times10^{-10}$ | $1.01\times10^{-6}$ | |
| 6q15 | 91474473 | rs713155 | 0.3966 | 274 | 345 | 121 | 7296 | $3.11\times10^{-10}$ | $5.08\times10^{-7}$ | |
| 1p35.1 | 34020651 | rs476463 | 0.1203 | 567 | 168 | 5 | 1472 | $3.18\times10^{-10}$ | $1.27\times10^{-6}$ | *CSMD2* |
| 7q31.32 | 121989829 | rs2429582 | 0.3417 | 319 | 331 | 86 | 2496 | $4.23\times10^{-10}$ | $6.46\times10^{-7}$ | *CADPS2* |
| 3p21.31 | 46314816 | rs9990343 | 0.4811 | 197 | 374 | 169 | 2048 | $5.34\times10^{-10}$ | $4.41\times10^{-7}$ | |
| 11q23.3 | 115803577 | rs490592 | 0.2149 | 450 | 255 | 29 | 14528 | $1.39\times10^{-9}$ | $1.32\times10^{-6}$ | |
| 20q13.12 | 43557937 | rs11696501 | 0.1935 | 480 | 232 | 27 | 768 | $1.41\times10^{-9}$ | $8.54\times10^{-7}$ | *WFDC2, SPINT3* |
| 3p12.1 | 84563758 | rs10511089 | 0.1095 | 589 | 140 | 11 | 1664 | $1.79\times10^{-9}$ | $6.57\times10^{-7}$ | |
| 8q23.1 | 108858992 | rs4534106 | 0.3007 | 367 | 301 | 72 | 1984 | $2.27\times10^{-9}$ | $1.00\times10^{-6}$ | *BG436399* |
| 6q12 | 67705937 | rs11970254 | 0.3464 | 293 | 358 | 72 | 1024 | $2.29\times10^{-9}$ | $6.21\times10^{-7}$ | |
| 9p13.1 | 38030095 | rs7025303 | 0.4061 | 263 | 347 | 124 | 768 | $2.30\times10^{-9}$ | $1.21\times10^{-6}$ | *SHB* |
| 1p36.13 | 19441559 | rs710865 | 0.3824 | 277 | 354 | 103 | 256 | $2.65\times10^{-9}$ | $1.10\times10^{-7}$ | *KIAA0090, MRTO4, AKR7L* |
| 9p13.1 | 38031142 | rs7873102 | 0.3821 | 283 | 340 | 109 | 832 | $2.96\times10^{-9}$ | $6.42\times10^{-7}$ | *SHB* |
| 20p12.1 | 12822585 | rs2073233 | 0.4291 | 234 | 369 | 131 | 2560 | $3.17\times10^{-9}$ | $1.42\times10^{-6}$ | *BC036700* |
| 2q37.3 | 242151629 | rs12479254 | 0.4049 | 255 | 341 | 119 | 1408 | $3.88\times10^{-9}$ | $5.70\times10^{-7}$ | *BOK, THAP4* |
| 16p12.1 | 24439219 | rs11643520 | 0.1160 | 574 | 146 | 11 | 1920 | $4.39\times10^{-9}$ | $6.06\times10^{-7}$ | *RBBP6* |
| 5p12 | 44222425 | rs4296809 | 0.1448 | 539 | 177 | 17 | 12736 | $4.41\times10^{-9}$ | $8.75\times10^{-7}$ | *BG334794* |
| 13q32.2 | 97764318 | rs688872 | 0.3804 | 283 | 345 | 106 | 3392 | $4.68\times10^{-9}$ | $1.06\times10^{-6}$ | *FARP1* |
| 14q22.1 | 51080549 | rs7140150 | 0.4566 | 219 | 353 | 160 | 1856 | $5.78\times10^{-9}$ | $4.77\times10^{-7}$ | *FRMD6* |
| 6p12.3 | 49596867 | rs9473582 | 0.3973 | 274 | 339 | 121 | 4416 | $5.98\times10^{-9}$ | $8.25\times10^{-7}$ | *GLYATL3* |